INVESTIGATIONS OF A SHEET MODEL FOR A BOUNDED PLASMA WITH MAGNETIC FIELD AND RADIATION

by

A. B. Langdon and J. M. Dawson

Memorandum No. ERL-M-257

1 January 1969

ELECTRONICS RESEARCH LABORATORY

College of Engineering
University of California, Berkeley
94720

ABSTRACT

A number of extensions are made to the usual one-dimensional sheet model for a plasma. The sheets, which lie in the y-z plane, are allowed to move in the x-y directions, passing freely through one another. The motion in the x direction produces the usual electrostatic field E_x, while the motion in the y direction produces retarded radiation fields E_y and B_z which are included in the calculation. A static external magnetic field in the z direction is included, and the smoothed-out stationary neutralizing background charge density varies with x.

Physical properties of this model are discussed. Expressions are derived for the synchrotron radiation from a gyrating sheet and the thermal radiation on the discrete space-time grid (used in the computer code). Dispersion properties of electromagnetic waves in the hot magnetized slab are discussed. Some peculiar aspects of the retarded radiation fields in one dimension are reconciled with the retarded fields from an extended body in three dimensions. The coupling of oscillations of the bounded slab to the field outside is discussed.

A computer code has been written to follow the model in time from some initial state. Measurements are presented and discussed of sheet drag and of the spectrum of emitted radiation when the model is near equilibrium.

TABLE OF CONTENTS

LIST OF FIGURE TITLES

I. Introduction

A great deal of information about the detailed kinetics of high temperature plasmas has been obtained in the last few years from simplified models of plasmas which can be solved numerically on large digital computers. Most of this has been done with one-dimensional models of bounded or periodic plasmas, with no magnetic field. We would like to be able to extend these useful techniques to study radiation processes and kinetic theory of bounded magnetized plasmas. A model has been proposed (1,2) which includes these effects for a simple geometry without losing too much of the computational simplicity of the electrostatic sheet model. This work will develop some of the basic properties of this model, and will discuss some results of the calculations for near-equilibrium cases.

II. Description and Basic Properties of the Model

We begin by describing the model in some detail.

II.1 The Geometry. The Electrostatic Fields.

We have a fixed smooth backround charge distribution $-\sigma n_0(x)$. This may be an arbitrary function, but in the work to be described here,

$$\begin{aligned} n_0(x) &= 0 \qquad\qquad \text{for } |x| > R \\ &= n_0 \text{ constant} \quad \text{for } |x| \leq R \end{aligned} \qquad \text{II.1.1}$$

Charge sheets are placed in this system, with their faces normal to the x axis. The quantities σ and m are the surface charge and mass densities for a sheet. The sheets move in the x-y plane, passing freely through each other and through or outside the backround charge. No collisional effects of the type used in (3) are added at crossings. The electrostatic field may be obtained from Poisson's equation

$$\frac{\partial E_x}{\partial x} = 4\pi\sigma\left[n(x,t) - n_0(x)\right] \qquad \text{II.1.2}$$

$$n(x,t) = \sum_s \delta(x - x_s(t))$$

If the sheets are displaced from their electrostatic equilibrium positions but remain inside the slab, each sheet experiences a restoring acceleration

$$-\omega_p^2 = (x - x_0)$$

where $\omega_p^2 = 4\pi n_0 \sigma^2/m$ and x_0 is the equilibrium position for the sheet. Thus the cold (noncrossing) oscillations consist of independent vibrations at the local plasma frequency ω_p. So far we have not departed from the usual sheet model, except perhaps for the boundedness. These sheet models have been analyzed by several authors (4,5,6).

II.2 Addition of Static Magnetic Field.

We now add a static magnetic field, B_{0z}, which lies in the plane of the slab. In this work, this magnetic field will be uniform. For cold

(noncrossing) electrostatic oscillations inside the slab we have

$$\ddot{x} = -\omega_p^2 (x - x_0) + \omega_c \dot{y} \qquad \text{II.2.1a}$$

$$\ddot{y} = -\omega_c \dot{x} \qquad \text{II.2.1b}$$

where $\omega_c = \sigma B_0/(mc)$.

There is an immediate first integral of the sheet equations of motion in the electrostatic case. We find that the y component of the sheet canonical momentum $m(\dot{y}+\omega_c x)$ is conserved. Alternatively, we can say that the x component of the guiding center $x_{gc} = x + \dot{y}/\omega_c$ is a constant. Note this is also true in a hot plasma because II.2.1b still holds during a crossing, and is approximately true when radiation is included. Thus all sheets remain within two or three Larmor radii of their original positions, since $\dot{y}$ will not change by more than two or three times $v_{th} = \sqrt{\text{av } v_x^2}$. This turns out to be important in several connections later.

A solution of eqns. II.2.1 is

$$x(t) = x_a + \alpha \cos \omega_h t + \beta \sin \omega_h t$$

$$y(t) = y_a + \frac{\omega_c}{\omega_h}\left(-\alpha \sin \omega_h t + \beta \cos \omega_h t\right) \qquad \text{II.2.2}$$

where $\omega_h^2 = \omega_p^2 + \omega_c^2$ and α, β, x_a and y_a depend on the initial conditions:

$$\alpha = \frac{\omega_p^2}{\omega_h^2}(x(0) - x_a) - \frac{\omega_c}{\omega_h^2}\dot{y}(0)$$

$$\beta = \frac{1}{\omega_h}\dot{x}(0)$$

$$x_a = x(0) - \alpha$$

$$y_a = y(0) - \frac{\omega_c}{\omega_h^2}\dot{x}(0) + \frac{\omega_p^2}{\omega_c}(x_a - x_0)t$$

we can also write the position as

$$x = x_a - \frac{1}{\omega_c}(\dot{y} - \dot{y}_a)$$

$$y = y_a + \frac{\omega_c}{\omega_h^2}\dot{x}$$

which shows that x_a and y_a are the non-oscillating parts of x and y.

Thus the sheet motion is a constant "E × B" drift in the y direction due to the average electrostatic force, superimposed on an elliptical oscillation at the hybrid frequency ω_h, whose ratio of x and y axes is ω_h/ω_c.

Consider a uniform hot sheet plasma in which orbit phases are randomly distributed and there are many crossings per oscillation period. The electrostatic force remains small compared to the $\underline{v} \times \underline{B}_0$ force, and is no longer strongly correlated with sheet position. Therefore the average sheet motion is nearly in circles at the cyclotron frequency. However let us consider $n_0 L$ sheets whose guiding centers lie in an interval of length L, with center of mass at $(\bar{x},\bar{y})$. This group exerts no net force on itself through the electrostatic field. The acceleration of its center of mass due to the backround charge and the magnetic field is $-\omega_h^2(\bar{x} - \bar{x}_0)$. The force due to the electrostatic field of sheets not included in the group changes by $4\pi\sigma^2$ every time an "outside" sheet crosses one of our group; the number of sheets involved is $\sim n_0 R_L = n_0 v_{th}/\omega_c$ and the average depth of interpenetration is $\sim R_L$, so this acceleration of the center of mass is $\sim (n_0 R_L)^2 4\pi\sigma^2/(n_0 Lm) = R_L^2\omega_p^2/L$. If L is large, this latter acceleration is unimportant and the center of mass moves in the same way as did a single sheet in non-crossing motion. The amplitude of the center of mass oscillation is small compared to R_L in this picture but can be significant if a long wavelength wave is excited.

The dielectric function for an infinite uniform Vlasov plasma with a Maxwellian velocity distribution and with fields varying as $\exp(i\,\underline{k}\cdot\underline{x} - i\,\omega t)$, where $\underline{k}$ is perpendicular to $\underline{B}_0$, is (the calculation is almost identical to those in ref. 7 and 8 for point particle plasmas)

$$K_{xx} = 1 - 2\omega_p^2 \frac{e^{-\lambda}}{\lambda} \sum_{q=1}^{\infty} \frac{q^2 I_q(\lambda)}{\omega^2 - (q\omega_c)^2}$$

$$\lambda = \frac{k^2 V_{th}^2}{\omega_c^2} \qquad \text{I.2.3}$$

The solutions of $K_{xx}=0$ are sometimes called the Bernstein modes. Plots of these solutions appear several times in the literature, see for example ref. 9.

II.3 The Model With Radiation

The radiation fields, like everything else, depend only on x and t. The quantities v_z, E_z and B_y will remain zero if set so initially. Such is the case in all these calculations. The complete set of equations to be solved is then

$$\frac{\partial B_z}{\partial x} + \frac{1}{c}\frac{\partial E_y}{\partial t} = -\frac{4\pi}{c} J_y \qquad \text{II.3.1a}$$

$$\frac{\partial E_y}{\partial x} + \frac{1}{c}\frac{\partial B_z}{\partial t} = 0 \qquad \text{II.3.1b}$$

$$J_y(x,t) = \sigma \sum_s \dot{y}_s(t)\, \delta(x - x_s(t)) \qquad \text{II.3.2}$$

$$\dot{p}_x = \sigma E_x + \omega_c' p_y \qquad \text{II.3.3a}$$

$$\dot{p}_y = \sigma E_y - \omega_c' p_x \qquad \text{II.3.3b}$$

$$\omega_c' = \sigma (B_z + B_0)(p^2 + m^2c^2)^{-\frac{1}{2}} \qquad \text{II.3.3c}$$

together with II.1.1-2.

It is convenient to rewrite the radiation equations II.3.1 in this physically appealing manner:

$$\left(\pm\frac{\partial}{\partial x} + \frac{1}{c}\frac{\partial}{\partial t}\right) E_{R\atop L} = -\frac{2\pi}{c} J_y \qquad \text{II.3.4}$$

where $E_{R\atop L} = \frac{1}{2}(E_y \pm B_z)$ II.3.5

E_R and E_L are the electric fields associated with right and left going energy. We integrate these equations along their characteristics to get the retarded solutions

$$E_{R\atop L} = \mp\frac{2\pi}{c}\int_{\mp\infty}^{x} dx'\, J_y\left(x', t - \frac{1}{c}|x-x'|\right)$$

from which we get*

$$E_y(x,t) = -\frac{2\pi}{c}\iint dx'dt'\, \delta\left(t-t'-\frac{1}{c}|x-x'|\right) J_y(x',t')$$

$$B_z(x,t) = -\frac{2\pi}{c}\iint dx'dt'\, \delta\left(t-t'-\frac{1}{c}|x-x'|\right) J_y(x',t')\, \mathrm{sgn}(x-x') \qquad \text{II.3.6}$$

For a single sheet $J_y(x',t') = \sigma \dot{y}_s(t') \delta(x'-x_s(t'))$ and these give

$$E_y(x,t) = -2\pi\sigma \frac{\dot{y}_s(t')/c}{1-\mathrm{sgn}(x-x_s(t'))\,\dot{x}_s(t')/c} \qquad \text{II.3.7}$$

where $t-t' = \frac{1}{c}\left|x-x(t')\right|$. We can understand this physically more easily by considering a sheet of finite but small thickness Δ. According to II.3.4 the rate of change of the radiation field E_R as it moves to the right is $\frac{dE}{dt}R = -2\pi J_y$. The time taken for the radiation to cross the sheet is $\Delta/(c-v_x)$ and the current inside the sheet is $\sigma v_y/\Delta$. Thus the change in E_R is $-2\pi(\sigma v_y/\Delta)(\Delta/(c-v_x))$ in agreement with II.3.7.

Consider a sheet with $\dot{x}_s=0$. Then $E_y=-2\pi\Delta\dot{y}_s(t-\frac{1}{c}|x-x_s|)/c$. The radiation drag on the sheet is $\sigma E_y=-2\pi\sigma^2\dot{y}_s/c$ leading to a velocity decay with e-folding time $\tau_r=mc/(2\pi\sigma^2)$. This will be long compared to a plasma period ($\omega_p\tau_r = 2n\lambda_D/(v_{th}/c)$. Note that $\omega_p\tau_r \to \infty$ as we go to the Vlasov limit $n\lambda_D \to \infty$).

Note that the radiation fields and the drag are proportional to the velocity instead of the acceleration as is the case for a point particle in 3-d. Perhaps a simple example will relieve the suspicion with which this result is usually received. Consider a spherical shell of radius R and total charge $q=4\pi R^2\sigma$. Let its center oscillate about the origin with velocity $\underline{v}(t)=\underline{V}\sin\omega t$. To first order in V/c the vector potential outside the sphere is in the Lorentz gauge

$$\underline{A}(r,t) = -4\pi R^2\sigma \frac{\underline{V}}{c} \frac{\sin kR}{kR} \frac{\sin(kr-\omega t)}{r}$$

$$k = \omega/c$$

from which

$$\underline{B}(\underline{x},t) = -4\pi R^2\sigma\, \hat{r}\times\frac{\underline{V}}{c}\frac{\sin kR}{kR}\left[-\frac{\sin(kr-\omega t)}{r^2}+k\frac{\cos(kr-\omega t)}{r}\right]$$

In the limit $R \to 0$ with q constant we have the point particle result.

Now consider the magnetic field as $R \to \infty$ holding q and r-R constant, which approaches the case of an infinite sheet with an observer nearby.

$$\underline{B}(\underline{x},t) = -4\pi\sigma\,\hat{r} \times \frac{V}{c} \lim_{R\to\infty} R^2 \frac{\sin kR}{kR}\left(-\frac{\sin(kR-\omega t')}{r^2} + \frac{k}{r}\cos(kR-\omega t')\right)$$

$$= -2\pi\sigma\,\hat{r} \times \frac{V}{c} \sin\omega t'$$

$$t' = t - \frac{r-R}{c}$$

The radiation field is proportional to the retarded velocity V sin $\omega t'$ and is the same as we get for an infinite sheet with normal $\hat{r}$ and at a position $\hat{r}(r-R)$ from a point on its surface.

Also consider the radiation field energy as $\omega \to \infty$.

$$\lim_{\omega\to\infty} \frac{1}{2T} \int_{-T}^{T} dt\, B^2(\underline{x},t) = \lim_{k\to\infty} \left|2\pi\sigma\,\hat{r} \times \frac{V}{c} \frac{R}{k} \sin kR\right|^2 \left(\frac{1}{r^4} + \frac{k^2}{r^2}\right)$$

$$= \frac{1}{2}\left|2\pi\sigma\,\hat{r} \times \frac{V}{c} \frac{R}{r}\right|^2$$

again indicating velocity-proportional ($\propto V$ rather than $\propto \omega V$) fields when the shell is many wavelengths across.

*B_z is the Biot-Savart field with retardation.

II.4 The Dielectric Tensor and Wave Propagation.

The cold fluid plasma dielectric tensor is

$$K_{xx} = K_{yy} = 1 - \frac{\omega_p^2}{\omega^2 - \omega_c^2}$$

$$K_{xy} = -K_{yx} = -i \frac{\omega_c}{\omega} \frac{\omega_p^2}{\omega^2 - \omega_c^2} \qquad \text{II.4.1}$$

The resulting dispersion relation is

$$c^2 k^2 = \frac{(\omega^2 - \omega_+^2)(\omega^2 - \omega_-^2)}{\omega^2 - \omega_h^2}$$

$$\omega_+ \omega_- = \omega_p^2$$

$$\omega_+ - \omega_- = \omega_c \qquad \text{II.4.2}$$

The dielectric tensor for an infinite uniform Vlasov gas of sheets with a Maxwellian distribution of velocities is (again following ref. 7 or 8)

$$K_{xy} = -K_{yx} = 2\omega_p^2 \frac{\omega_c}{\omega} e^{-\lambda} \sum_1^\infty \frac{iq^2 (I_q - I_q')}{\omega^2 - (q\omega_c)^2}$$

$$K_{yy} = K_{xx} - 4\omega_p^2 \lambda e^{-\lambda} \left[\sum_1^\infty \frac{I_q - I_q'}{\omega^2 - (q\omega_c)^2} + \frac{I_0 - I_0'}{2\omega^2} \right] \qquad \text{II.4.3}$$

with K_{xx} and λ given by II.2.3. The dispersion relation is

$$0 = \begin{vmatrix} K_{xx} & K_{xy} \\ K_{yx} & K_{yy} - \frac{c^2 k^2}{\omega^2} \end{vmatrix} \qquad \text{II.4.4}$$

Figures II.3-10 are solutions of this dispersion relation. There are three cases shown, in which $\omega_+ < 2\omega_c$, $\omega_h < 2\omega_c < \omega_+$ and $\omega_- < 2\omega_c < \omega_h$. These solutions have real ω for real k for the same reason as in the electrostatic case. The solutions are considerably more complicated and numerous (there are normally 2 between adjacent cyclotron harmonics) than those of the electrostatic relation and bear little resemblance to

them except of course for the Bernstein modes which are almost longitudinal at large k. The number of modes can be "explained": involving J_y as well as J_x doubles the number of degrees of freedom and hence the number of modes. Then two more modes are added corresponding to the transverse degrees of freedom.

One interesting feature in common with the electrostatic case is that no solution ever crosses any harmonic of the cyclotron frequency, including the first (fundamental). This leads to interesting behavior at a harmonic which the solution of the cold plasma dispersion relation does cross. The hot solution comes very close to the harmonic and then turns sharply off to k=0 on one side of the harmonic and $k=\infty$ on the other, keeping very close to the harmonic (frequencies closer than $.001\omega_c$ to a harmonic are not shown in figures II.3-8. See figures II.9-10). These waves are circularly polarized and interact strongly with the plasma because the frequency is so near an exact resonance of the particle motion.

The dispersion relation has also been solved when a relaxation term $-\nu f_1$ has been added to the Vlasov equation (Appendix I). The results are unsurprising. Two new modes near $\omega=0$ are added. For real k the modes near harmonics are damped at nearly the relaxation rate ν due to the wave energy being mostly in the particles. The spatial damping rate is very large for these modes, as may be inferred from the argument that a wave packet is temporally damped at the rate Im ω while moving with the (very small) group velocity. Another argument is that if $k=k_0$, $\omega=\omega_0-i\gamma$ is a solution of the dispersion relation then so is $k\approx k_0+i\gamma/(\partial\omega/\partial k)$, $\omega=\omega_0$.

II.5 Single Sheet Synchrotron Radiation

Let us calculate the radiation from a single gyrating sheet, with

$$x_s = \frac{v}{\omega_c} \sin \omega_c t$$

$$\dot{y}_s = - v \sin \omega_c t$$

The corresponding current density is

$$J_y (x', t') = - \sigma v \sin \omega_c t' \, \delta \left(x' - \frac{v}{\omega_c} \sin \omega_c t' \right)$$

The resulting radiation electric field is from II.3.6

$$E_y (x, t) = 2\pi \sigma \frac{v}{c} \iint dx' dt' \, \delta \left(t - t' - \frac{1}{c} |x - x'| \right) \sin \omega_c t' \, \delta \left(x' - \frac{v}{\omega_c} \sin \omega_c t' \right)$$

$$= 2\pi \sigma \frac{v}{c} \int dt' \, \delta \left(t - t' - \frac{1}{c} \left| x - \frac{v}{\omega_c} \sin \omega_c t' \right| \right) \sin \omega_c t'$$

We now place the observer outside the sheet's orbit, i.e. $|x| > |v/\omega_c|$, whence

$$E_y (x, t) = 2\pi \sigma \frac{v}{c} \int dt' \, \delta \left(t - \frac{|x|}{c} - t' + \frac{v}{c\omega_c} sgn(x) \sin \omega_c t' \right) \sin \omega_c t'$$

In terms of frequency

$$E_y (x, \omega) \equiv \int dt \, e^{i\omega t} E_y (x, t)$$

$$= 2\pi \sigma \frac{v}{c} e^{i \frac{\omega}{c} |x|} \int dt' \sin \omega_c t' \exp \left(i\omega t' - i \frac{\omega}{\omega_c} \frac{v}{c} sgn(x) \sin \omega_c t' \right)$$

Using the identity $\exp (iz \sin \theta) = \sum_{p=-\infty}^{\infty} J_p (z) \, e^{ip\theta}$ we get

$$E_y (x, \omega) = (2\pi)^2 i \sigma \frac{v}{c} \sum \exp \left(ip \omega_c \frac{|x|}{c} \right) J_p \left(p \frac{v}{c} sgn(x) \right) \delta (\omega - p\omega_c) \qquad \text{II.5.1}$$

or

$$E_y (x, t) = 4\pi \sigma \frac{v}{c} \sum_{p=1}^{\infty} J_p' \left(p \frac{v}{c} sgn(x) \right) \sin p\omega_c \left(t - \frac{|x|}{c} \right) \qquad \text{II.5.2}$$

This derivation is simple mathematically and contains no approximation but it obscures the physics somewhat. To see the two effects which contribute equally to the 2nd harmonic emission, we go back to eqn. II.3.7.

Consider the case $x > |v/\omega_c|$, for which $\mathrm{sgn}(x-x_s)=1$

$$\omega_c t' = \omega_c (t-\tfrac{x}{c}) + \tfrac{v}{c} \sin \omega_c t'$$

$$= \omega_c (t-\tfrac{x}{c}) + \tfrac{v}{c} \sin\left[\omega_c (t-\tfrac{x}{c}) + \tfrac{v}{c} \sin \omega_c t'\right]$$

$$= \omega_c (t-\tfrac{x}{c}) + \tfrac{v}{c} \sin \omega_c (t-\tfrac{x}{c}) + \theta(\tfrac{v}{c})^2$$

Now we can write

$$E_y (x,t) = 2\pi\sigma \tfrac{v}{c} \sin\left[\omega_c (t-\tfrac{x}{c}) + \tfrac{v}{c} \sin \omega_c (t-\tfrac{x}{c})\right]\left[1-\tfrac{v}{c}\cos(\omega_c t-\tfrac{x}{c})\right]^{-1} + \theta(\tfrac{v}{c})^3$$

$$= 2\pi\sigma \tfrac{v}{c} \sin \omega_c (t-\tfrac{x}{c}) \left[1+\tfrac{v}{c}\cos \omega_c (t-\tfrac{x}{c})\right]^2 + \theta(\tfrac{v}{c})^3$$

One of the brackets is due to the oscillating phase in $\dot{y}_s$, the other is from the denominator in II.3.7. We see both make the same contribution to this approximation. We get

$$E_y (x,t) = 2\pi\sigma \tfrac{v}{c} \left[\sin \omega_c (t-\tfrac{x}{c}) + \tfrac{v}{c} \sin 2\omega_c (t-\tfrac{x}{c})\right] + \theta(\tfrac{v}{c})^3$$

which is consistent with II.5.2.

The time averaged Poynting flux is

$$\bar{P}_x (x,t) = \frac{c}{4\pi} \overline{E_y^2}\, \mathrm{sgn}(x) = \frac{\pi}{2}\sigma^2 c \left[(\tfrac{v}{c})^2 + (\tfrac{v}{c})^4\right]$$

The terms are associated with frequencies ω_c and $2\omega_c$ respectively, higher harmonics are neglected. The total radiation rate, after averaging over a Maxwellian velocity distribution, is $\dot{W}_R = 2\pi\sigma^2 c\left[(\tfrac{v_{th}}{c})^2 + 4(\tfrac{v_{th}}{c})^4\right]$ or $\frac{1}{\omega_p}\frac{\dot{W}_B}{W_R} = \frac{1}{2}\frac{1}{n\lambda_D}\frac{v_{th}}{c}\left(1+4(\tfrac{v_{th}}{c})^2\right)$ this expression also holds for a group of sheets radiating incoherently.

II.6 Thermal Equilibrium of the Radiation Field

Let us consider first the continuum case. If we take a vacuum of length L with perfectly conducting walls, there will be independent standing waves with wavelength λ_1 and frequency f_1.

$$\lambda_l = \frac{2L}{l} = \frac{c}{f_l}$$

In unit frequency interval there are 2L/c modes. Associated with each mode and our one polarization, there is an energy θ divided between the electric and magnetic fields. We find for the energy density U

$$dU = \frac{2\theta}{c}\, df \qquad f > 0$$

The net flux in one direction at some point is $\theta\, df$ since half goes each way.

This classical result suffers from the usual "ultraviolet catastrophe" due to the infinite number of degrees of freedom of the continuum. We will see that classical statistics works fine for our discrete system with its finite number of degrees of freedom.

The fields E_R and E_L are given at N discrete points in space, separated by $\Delta x = L/N$. The energy in the radiation field is

$$W = \frac{\Delta x}{8\pi} \sum_0^{N-1} \left\{ (E_{R,k} + E_{L,k})^2 + (E_{R,k} - E_{L,k})^2 \right\}$$

$$= \frac{\Delta x}{4\pi} \sum_0^{N-1} \left(E_{L,k}^2 + E_{R,k}^2 \right)$$

We see immediately that we have 2N degrees of freedom and that in thermal equilibrium

$$\frac{\Delta x}{4\pi}\, \overline{E_{L}^2}_{R} = \frac{\theta}{2} \qquad U = \frac{N\theta}{L} = \frac{\theta}{\Delta x}$$

This says nothing about the frequency and wavelength properties of the radiation. It is convenient to define

$$E_k = -E_{L,N-k} \qquad k = 0,1..N-1$$
$$= E_{R,k-N} \qquad k = N..2N-1$$

With perfectly conducting walls at both ends, the radiation evolves according to

$$E_k(t-\Delta t) = E_{k-1}(t)$$

with k defined modulo 2N. We now define

$$\tilde{E}_l = \frac{1}{2N}\sum_{k=0}^{2N-1} E_k \exp\left(2\pi i \frac{kl}{2N}\right)$$

whence

$$E_k = \sum_{l=0}^{2N-1} \tilde{E}_l \exp\left(-2\pi i \frac{kl}{2N}\right)$$

which separates the fields into independent modes sinusoidal in space and time. The frequency of mode l is lc/(2L) and the wavelength is 2L/l. Only half the $\tilde{E}_l$ are independent; since E_k is real, $\tilde{E}_l^* = \tilde{E}_{2N-l}$. The radiation energy may be rewritten

$$W = \frac{\Delta x}{2\pi}\sum_{0}^{2N-1} E_k^2 = \frac{L}{2\pi}\left\{\tilde{E}_0^2 + \sum_{l=1}^{N-1}\left[(\mathrm{Re}\,\tilde{E}_l)^2 + (\mathrm{Im}\,\tilde{E}_l)^2\right] + \tilde{E}_N^2\right\}$$

so the energies in the various frequencies are

$$\frac{\theta}{2} \quad \text{for} \quad f = 0 \quad \text{and} \quad f = \frac{c}{2\Delta x}$$

$$\theta \quad \text{for} \quad f = \frac{cl}{2L}, \quad l = 1..N-1$$

The spectrum of the radiation is, for large L

$$dU = \frac{2\theta}{c}\,df \qquad 0 < f < \frac{c}{2\Delta x}$$
$$= 0 \qquad \text{otherwise}$$

The total energy density is $\int_0^{\frac{c}{2\Delta x}} df \frac{dU}{df} = \frac{\theta}{\Delta x}$ as we found earlier.

The physical meaning of the Nyquist frequency $c/(2\Delta x) = 1/(2\Delta t)$ is that any frequency above the Nyquist frequency is indistinguishable from some frequency below the Nyquist frequency. In all the computer runs $\omega_h \Delta t/(2\pi) \lesssim .008$.

II.7 Remaining Theoretical Problems

In this section we relate some difficulties encountered in attempting a theoretical description of the kinetic theory of this system.

A powerful tool in the kinetic theory of plasmas is the dressed test-particle picture; see e.g. reference 9 for many applications. Let us see what happens when one tries to do such a calculation for this system. One begins by finding the current density due to uncorrelated unscreened sheets moving in the unperturbed fields. If we consider a system without boundaries these unperturbed orbits are circles described at the cyclotron frequency. Because we have no space variation parallel to the imposed magnetic field, there can be no Doppler shift even if the sheets do move parallel to this field, and thus the only frequencies present in the current density of the unscreened test sheets are the cyclotron frequency and its harmonics. One then goes on to calculate the linear response of a Vlasov gas to this current density which, because of the linearity, will also only contain frequencies which are the cyclotron frequency and its harmonics. This will be true for all quantities derived by such methods, such as the spectrum of electrostatic field fluctuations.

For comparison let us calculate the spectrum using the fluctuation-dissipation theorem, which gives (ref. 9, eqn. 4.54)

$$\frac{1}{8\pi}\langle E_x^2\rangle = -\int \frac{dk}{2\pi}\,\frac{\theta}{2\pi\omega}\,\mathrm{Im}\,K_{xx}^{-1}(k,\omega)$$

where $\theta = mv_{th}^2$. The quantity Im K_{xx}^{-1} (with K_{xx} given by I.2.3) appears at first glance to be zero for real k and ω, but it can have terms $\delta(\omega-\omega_j(k))$ at the roots of $K_{xx}=0$, which are real*, and will still satisfy $K_{xx}K_{xx}^{-1}=1$. The correct result, obtained by the causality requirement that K_{xx}^{-1} be

analytic in the upper half ω plane (or by adding a little damping) is

$$\mathrm{Im}\, K_{xx}^{-1}(k,\omega) = \mathrm{Im} \lim_{\epsilon \to +0} \frac{1}{K_{xx}(k,\omega+i\epsilon)} = -\pi \sum_j \frac{\delta(\omega-\omega_j(k))}{\frac{\partial K_{xx}(k,\omega_j)}{\partial \omega_j}}$$

The fluctuation energy is therefore

$$\frac{1}{8\pi} \langle E^2 \rangle = \int \frac{dk}{2\pi}\, d\omega\, \frac{\theta}{2} \sum_j \frac{\delta(\omega-\omega_j(k))}{\omega_j \frac{\partial K_{xx}(k,\omega_j)}{\partial \omega_j}}$$

summed over the Bernstein modes (both positive and negative frequencies). Thus we find the spectrum is large for any k and ω which satisfy the electrostatic dispersion relation, as we would expect after seeing that the center of mass of a large group of sheets oscillates at the hybrid frequency. We do not now fully understand the difficulty in this geometry with the test particle picture.

Another interesting feature of the model is that a gyrating sheet comes into contact with mostly the same other sheets (because x_{gc} is nearly constant). Any disturbance it causes in the motion of another sheet it will see again and again as it rapidly re-crosses this sheet. This contrasts with a 3-d point-particle plasma in which charges move along the magnetic field encountering new particles all the time. Thus the Markovian character of particle interactions in a real plasma is absent here, posing additional statistical difficulties.

*We can see from the form of K_{xx} that for real k if ω is a root then ω^* is also a root. Unless ω is real we have a growing mode which is impossible with our Maxwellian velocity distribution. The damping of an initial disturbance when ω_c is small is due to phase mixing of the Bernstein modes (10) similiar to the phase mixing of the Van Kampen undamped electrostatic modes of an unmagnetized plasma (11).

III. Remarks on the Numerical Solution

The equations II.3.1 for E_y and B_z are awkward to integrate by the usual finite difference methods, because J_y is not a smooth function and E_y is needed at least as accurately near the radiating sheet as far from it. However it is easy to integrate accurately the equations II.3.4 for E_L and E_R. If we set up a grid in x-t space such that $\Delta x = c\,\Delta t$, then at each time step (for $J_y=0$) we simply move the E_R field values one unit to the right and the E_L values one unit to the left. Where the field values cross a sheet they jump in value by

$$\Delta E_{R\atop L} = -2\pi\sigma \frac{\dot{y}/s}{1 \mp \dot{x}/c} \qquad \text{III.1}$$

In the work to be described here, the equations are solved in a nonrelativistic approximation. This enables one to remove those effects whose mechanisms require relativity from the ones currently under study, and is somewhat faster computationally (but a fully relativistic solution is no great complication). Specifically, Newton's equations were used in nonrelativistic form, and the radiation magnetic field was not included in the Lorentz force. Note that the latter force has little net effect (in that $\underline{v} \times \underline{B}_1 \cdot \frac{\partial f}{\partial \underline{v}} = 0$) for a distribution isotropic in (v_x, v_y) and with $v_z=0$.

However the denominator in III.1 is included, although its contribution to the field is of order $(v/c)^2$ compared to that of E_x. This is because we wish the relative error in a quantity to be small compared to v/c. Neglecting the denominator would reduce the intensity of the 2nd harmonic emission from a gyrating sheet by a factor of 4 (see II.5). Also, this form conserves the total magnetic flux $\int B_z dx$, which is not true if the denominator is omitted.

Thus the equations to solved numerically are

$$\ddot{x}_s = \frac{\sigma}{m} E_x + \omega_c \dot{y}_s$$

$$\ddot{y}_s = \frac{\sigma}{m} E_y - \omega_c \dot{x}_s$$

together with II.1.1-2, II.3.2 and II.3.4-5. These equations conserve total system energy but not momentum (the radiation pressure on the sheets is incomplete).

This set of equations is solved as an initial-value problem, starting near thermal equilibirum in most cases (the sheets are in electrostatic equilibrium, the velocity distribution is Maxwellian, while $y_s=0$, $E_L=E_R=0$). This is not quite equilibrium (for instance sheet correlations are incorrect) and there are a couple of periods of chaos while things settle down. Normally the boundary conditions on the radiation fields are such that radiation freely leaves through the ends of the system and none enters.

Several quantities including the various energies are monitored during a computer run. The total energy shows a slow drift downward of less than .3% in a run of 200 plasma periods.

The sheet coordinates and velocities, radiation fields, etc. are recorded on tape about 10 times per plasma period during a run. Then the run may be reexamined at leisure without recomputing.

The model simulation program was written in Algol 60 (ALCOR implemention) and machine code for the IBM 7094 and 7044 at Princeton University.

IV. Drag On a Sheet

The drag on a sheet is an important quantity to measure, especially since it was not estimated theoretically (due to difficulties with the test sheet picture) for the magnetized case, and the results for the unmagnetized case (3,5) indicate a high damping rate; for a typical case in which $n\lambda_D = 3.8$ a slow sheet velocity e-folding time is about $3f_p^{-1}$ and a fast sheet loses speed by an amount v_{th} in a time $1.2\ f_p^{-1}$ (where "fast" and "slow" are relative to about $2.5v_{th}$). The same drag on a sheet in a magnetic field would give about twice this damping time due to the added energy associated with the motion in the y direction. However this is still a high damping rate.

Dawson's experimental measure of drag (3) may easily be generalized to the magnetized case as follows: We wish to know the motion in some averaged sense at times $t_0+\tau$ of a sheet for which $\underline{v}(t_0)=\underline{v}_0$. Since it will turn out that the motion is very nearly at the cyclotron frequency, and that therefore the motion is very nearly circular, we will be satisfied with not knowing the directions of $\underline{v}(t_0)$ and $\underline{v}(t_0+\tau)$ separately, but only the difference in direction. This may be expressed conveniently by defining for each sheet a complex velocity $v = v_x + i\ v_y$. We form

$$C(\tau) = \left\langle v^*(t_0)v(t_0+\tau)/\left|v(t_0)\right|^2 \right\rangle$$

where the average is taken over times t_0 such that $v(t_0) \approx v_0$ and over all sheets. (This is what the usual autocorrelation for a complex quantity will become if we restrict its ensemble average.)

This average was measured in two representative model runs differing only in the magnetic field. The parameters in the first run were

$f_p = 1.12\ f_c$

$\tau_r = 338\ f_p^{-1}$ so that radiation damping is not being seen here

$n\lambda_0 = 3.8$

Plots of the phase and modulus of $C(\tau)$ for $v_0 = .3v_{th}$ (figures IV.1-2) show the modulus decreasing roughly linearly and the phase changing very linearly. $C^*(\tau) = C(-\tau)$ as befits an almost reversible system (the only irreversibility is due to radiation leaving the system while none enters). The wiggle in these quantities is at about the cyclotron frequency and is probably due to the small linear drift in the y direction superimposed on the circular motion, which has been observed. The rotation rate of C is within 1 or 2% of the cyclotron frequency. This means that as expected the single sheet motion is very nearly circular, since the additional forces needed to flatten the circle into an ellipse would also increase the frequency. Measurements at other values of v_0 show the same behavior. For three different speeds v_0 we find

v_0/v_{th}	$f_p\lvert\tau\rvert/(1-C(\tau))$
.5	4.5
1.4	5.5
2.0	8.0

We see that the damping time is roughly constant for low v_0, increasing as we get up past v_{th}. This is like the unmagnetized drag, modified for the y motion as mentioned above.

In another run, the same as this except that $f_c = .6f_p$, again showed sheets rotate at frequency f_c and therefore move in circles. However now $|C(\tau)|$ decreases with $|\tau|$ somewhat more rapidly for small $|\tau|$ than large. The damping rate is the same within available accuracy as in the other case.

The physical meaning of the decay of $|C(\tau)|$ for $v_0 \approx v_{th}$ is as follows: The average of the magnitudes of the velocities would be expected to increase or decrease toward roughly the thermal speed. Therefore a decay in $|C|$ for slow sheets must be due primarily to a diffusion of gyration phases superimposed on the mean rotation at frequency ω_c.

V. The Observed Radiation Spectrum

One of the most interesting quantities to measure in the model numerical solutions is the frequency of the Poynting flux. Because there is often confusion about the relation of measurements made on discretized finite-length records to the "true" spectrum of a stationary process, we will spend a moment on an unusually simple formulation of the problem which is helpful when reading the time series literature.

V.1 The Statistical Problem

a The ensemble spectrum

We will use the Fourier transform conventions common in these discussions:

$$\hat{X}(f) = \int_{-\infty}^{\infty} dt\ e(-ft)\, X(t), \quad X(t) = \int_{-\infty}^{\infty} df\ e(ft)\, \hat{X}(f) \qquad \text{V.1.1}$$

where $e(x) = \exp(2\pi i x)$.

Transforming $E_y(t)$ and $B_z(t)$ (the x dependence will be omitted hereafter) and averaging over an ensemble

$$\langle E_y(t+\tfrac{\tau}{2})\, B_z(t-\tfrac{\tau}{2})\rangle = \int df\, df'\, e([f+f']t) \cdot e([f-f']\tfrac{\tau}{2})\, \langle \hat{E}_y(f)\, \hat{B}_z(f')\rangle$$

If the ensemble is stationary in time this must be independent of t, i.e. the derivative with respect to t of the above is zero, which requires

$$0 = (f+f')\, \langle \hat{E}_y(f)\, \hat{B}_z(f')\rangle$$

whose solution is of the form

$$\langle \hat{E}_y(f)\, \hat{B}_z(f')\rangle = \frac{4\pi}{c} P_x(f)\, \delta(f+f') \qquad \text{V.1.2}$$

This gives

$$C(\tau) \equiv \frac{c}{4\pi} \langle E_y(t+\tfrac{\tau}{2})\, B_z(t-\tfrac{\tau}{2})\rangle = \int df\, e(f\tau)\, P_x(f) \qquad \text{V.1.3}$$

from which follows

$$P_x(f) = \int d\tau\, e(-f\tau)\, C(\tau) \qquad \text{V.1.4}$$

Equation V.1.2 together with the case $\tau=0$ of V.1.3 suggest the interpretation of $P_x(f)$ as the frequency decomposition of the Poynting flux. Further examination of its properties shows that indeed Re $P_x(f)$ = Re $P_x(-f)$ is power in the usual sense, while Im $P_x(f)$ = - Im $P_x(-f)$ is a "reactive" power such as is found in a standing wave in one dimension.

b A spectral estimator

We wish to estimate $P_x(f)$ from a finite discrete sampling, i.e.

$$\left\{ E_y(t_i),\ B_z(t_i) \right\},\quad \left(i = 0, 1, \ldots N-1,\quad t_{i+1} - t_i = \Delta t \right)$$

for one realization from the ensemble. We could use

$$P_x'(f) = \Delta t \sum_{|l|<N} e(-f\Delta t)\, L(l\Delta t)\, \frac{1}{N-|l|} \sum_j E_y(t_j + l\Delta t)\, B_z(t_j) \qquad \text{V.1.5}$$

in which $0 \leq j < N-1$ for $l \geq 0$ and $1 \leq j < N$ for $l < 0$. The function $L(\tau)$, called the "lag window", controls the frequency resolution and reliability of the spectral estimates, as will be discussed below. To see the connection of P_x' with P_x we ensemble average P_x':

$$\langle P_x'(f) \rangle = \Delta t \sum_l e(-f\Delta t)\, L(l\Delta t)\, C(l\Delta t)$$

We may write the sum as being over all l if we require

$$L(\tau) = 0 \quad \text{for} \quad |\tau| \geq T < N\Delta t \qquad \text{V.1.6}$$

Then we can manipulate this expression into the form

$$\langle P_x'(f) \rangle = \int df'\, P_x(f') \sum_{l=-\infty}^{\infty} \hat{L}\left(f + \frac{l}{\Delta t} - f'\right) \qquad \text{V.1.7}$$

If $P_x(f)=0$ for $|f| > 1/(2\Delta t)$ and if the "spectral window" $\hat{L}(f)$ is peaked about f=0 with width $\delta f \ll 1/(2\Delta t)$, then

$$\langle P_x'(f) \rangle \simeq \int df\, P_x(f')\, \hat{L}(f-f')$$

for $|f| \lesssim \frac{1}{2\Delta t} - \delta f$

We choose L to be an even function with $L(0)=1$, so that $\hat{L}$ is real and $\int df\, L(f)=1$. From this expression we see that $\hat{L}(f)$ is like the frequency response of a laboratory receiver or spectrum analyser and δf is the passband width or resolution.

By making further assumptions about the ensemble, we can investigate the sampling variance of $P_x'(f)$ to see what affects its reliability. For instance, if the ensemble is Gaussian, we may express its 4th moments in terms of its 2nd moments and get an explicit expression for the covariance of P_x' in terms of P_x and $\hat{L}$ (see 12 or 13 for more details). The variance turns out to be inversely proportional to the resolution δf where P_x varies sufficiently slowly. If no window is used, the resolution is its smallest ($\approx 1/(N\Delta t)$) but the sampling variance of P_x' is as large as P_x' itself. This is intuitively reasonable when one remembers that a finite-length sample of a band-limited signal contains only a finite amount of information about P_x. This amount of information is not increased by sampling more often (decreasing Δt), or even continuously, if the maximum frequency of the signal is already less than the Nyquist frequency $1/(\Delta t)$ as we have earlier assumed.

A compromise must be made between resolution, sampling variance, the absence of "side lobes" in the spectral window, and the requirement of eqn. V.1.6. A convenient window is $\frac{3}{4}T\left(\frac{\sin \omega T/4}{\omega T/4}\right)$, usually called the Parzen window, which has small side lobes and is positive. This window is used in all the spectra shown here.

New methods have been developed recently for rapid computation of spectrum estimators for discrete time-series (14). These methods rely on the fast digital Fourier transform algorithm suggested by Tukey (15) and developed by the author and others (16, 17, 18).

V.2 Experimental Measurements

We will want to measure the Poynting flux spectrum inside the slab as well as outside. There might be some question about its measurement inside the orbit of a sheet. Every time the sheet crosses the measuring point the sign of B_z changes abruptly. Thus one might expect to see strong harmonics inside the slab just because we are inside the orbits of many sheets. However the main change in the 2nd harmonic content of B_z is out of phase with the 2nd harmonic content of E_y. Also the harmonic content of E_y is not much different inside the orbit than outside. These effects weaken the change in $P_x(2f_c)$.

In the plots the logarithm of $P_x(f)$ when it is positive (right-going power) is shown as a solid line, and the logarithm of minus P_x when it is negative (left-going power) is shown as a broken line. The power ratio from from the top of the plot to the bottom is 10,000 to 1. The power is normalized to the black-body level (section II.6) (the spectrum of radiation from a black body at the temperature of the slab would be plotted as unity for all frequencies). The frequency scale is in cycles per time step; full scale is $.0025\,\Delta t^{-1}$ in fig. V.1, and $.002\,\Delta t^{-1}$ thereafter.

It should be kept in mind that neither the black-body radiation spectrum nor the measured spectrum of the actual radiation is affected by the discrete space-time grid for frequencies below the Nyquist frequency (section II.6) which is always $0.5\,\Delta t^{-1}$ here.

Several runs were made with the model and spectra measured. It was found that the spectra in the early runs were rather amorphous. It is believed that this is due to the very low number of sheets per Debye length used at that time ($n\lambda_D=3.8$) which leads to the very large collision rate, as discussed in the last section. The damping washes out detail in the spectrum. The second case discussed below is a rerun of the most interesting

case with a slightly smaller damping rate ($n\lambda_D$=4.9) and more plasma periods giving somewhat improved results.

In the first case (Figs V.1) the physical parameters are

n_0=1.67 Δx^{-1} R=60 Δx v_{th}=.07 $\Delta x\ \Delta t^{-1}$ (c=1)

$\frac{\omega_p}{2\pi}$ = .005 Δt^{-1} $\frac{\omega_c}{2\pi}$ = .0029 Δt^{-1}

The spectrum is shown at a number of points inside and outside of the slab. The spectral window is $1500\Delta t\left(\frac{\sin 500\omega\Delta t}{500\omega\Delta t}\right)^4$. Outside the slab the spectrum shows a strong peak approaching black body level (80% on the left side, 65% on the right) at the hybrid frequency, which is also the 2nd harmonic of the cyclotron frequency. There are easily identifiable peaks at the third and fourth harmonics. The character of the spectrum outside the slab persists roughly as we enter a few Larmor radii into the slab. Thus the bulk of the radiation at each frequency is from the interior. (In looking at the spectra well inside the slab one should keep in mind that one is looking at the small difference of the much larger right and left going fluxes and not take too seriously the structure that appears.)

Although the spectrum does not reach black-body level at any frequency, the total radiation is only about 4% of what would be expected from cyclotron radiation from uncorrelated sheets (see II.5). The plasma arranges itself to keep the radiation down even below the black-body limit imposed by re-absorption.

A run with larger magnetic field yielded a very different spectrum. The parameters were

n_0=1.67 Δx^{-1} R=60 Δx v_{th}=.1 $\Delta x\ \Delta t^{-1}$

$\frac{\omega_p}{2\pi}$=.005 Δt^{-1} $\frac{\omega_c}{2\pi}$=.005 Δt^{-1}

In Figs. V.2 and V.3 the Poynting spectrum at various points is shown, first with spectral window $1875\left(\frac{\sin 625\,\omega\Delta t}{625\,\omega\Delta t}\right)^4$, then with a window half as wide. Outside the slab we find the intensity between cyclotron and hybrid frequencies is about as before, but now there is a strong peak at $2\omega_c$, and more prominent peaks at $3\omega_c$ and $4\omega_c$. The peak at $2\omega_c$ accounts for most of the radiated energy and would be even stronger if some of it were not being reabsorbed while crossing the slab (the outgoing flux reaches black-body level well within the slab and increases no further). The spectra inside the slab show that the harmonic radiation comes from the whole slab, not just the edges. It is a little difficult to estimate the rate of radiation at $2\omega_c$ because P_x includes the flux moving into the slab from the edges as well as that going out, and large energy fluxes are depleted by absorption, but the energy in the 2nd harmonic is about what one would expect from synchrotron radiation at this temperature (corresponding to about 2.5 kev. for an electron plasma).

A clue as to why the radiation at $2\omega_c$ is so much stronger in the 2nd case than the 1st is that the 2nd harmonic propagates, according to the cold dispersion relation, and does so for all lower ω_p. Whereas, in the 1st case, $2\omega_c$ is at the edge of a non-propagating band of frequencies, and enters this band when ω_p decreases.

It remains very interesting that the mechanism which keeps down the radiation near ω_h does not seem to apply to $2\omega_c$. A part of this question is the role of the radiation field in establishing the sheet correlations which produce this radiation. If it turned out that the radiation fields play no important role, the theoretical problem would be easier. A model run was made, identical to the 2nd case above except that after 10 plasma periods $\frac{q}{m} E_y$ was not included in integrating the sheet orbits. Thus radiation is

emitted by sheets but not reabsorbed, and there is no radiation drag. The resulting spectra are shown in Figs. V.4. $2\omega_c$, $3\omega_c$ etc. are about as before but ω_c is much stronger and ω_h is very strong. Evidently the radiation fields do have an important effect on the sheet correlations in this frequency range which characterizes the sheet motion. It may be that these low frequency modes radiate so well because of coherence (Appendix II) that energy cannot enter them fast enough to keep them at their thermal level. In that case we are not looking at a thermal plasma, and perhaps need a much larger system. But again, why does this not apply to $2\omega_c$? Perhaps the wavelengths associated with $2\omega_c$ are shorter and thus more effectively fed energy by the particles. Another possibility is that radiation at ω_h is always weak because it must tunnel through a cutoff region on its way out. This is less convincing since the cutoff region here is very small with our sharp-sided backround density.

VI. Summary and Conclusions

We have described a new computer sheet model for a magnetized plasma slab and the complete electromagnetic field. All gradients are perpendicular to the imposed magnetic field. Only the quasi-transverse extraordinary modes are excited.

First we develop the basic properties of the model, beginning with the electrostatic fields and their action on the sheet orbits when no crossing occurs. The mean motion of a group of sheets is found to be the same even if many sheet crossings occur as in the hot case, although on the average individual sheets move as though there were no electrostatic field if their gyration phases are random.

Some peculiar aspects resulting from $\underline{B}_0 \cdot \nabla = 0$ are mentioned. The fact that no average sheet motion is possible in the wave direction while all sheets oscillate across the waves with the same average frequency introduces a considerable difficulty into test-particle calculations and other kinetic theory problems. This is relieved if relativistic corrections are made to the particle orbits. Also the normal Markovian nature of particle interaction is lost since the sheets cannot get away from their neighbors. This feature raises novel unsolved problems in statistical mechanics.

Next the radiation fields are separated into left-going and right-going components. Surprisingly, the radiation from a sheet is found to be proportional to velocity instead of acceleration as is the case for 3-d point particles. However in an example of an oscillating charged spherical shell this velocity dependence is seen to be normal when the radiation wavelength is much smaller than the shell radius.

Solutions are presented of the dispersion relation for electromagnetic wave propagation in the nonrelativistic Vlasov limit. For the densities

($\omega_p \approx \omega_c$) and temperatures (around 2.5 kev.) of interest the hot quasistatic and cold electromagnetic approximations commonly used are found quite inadequate.

Returning to the single sheet we calculate exactly its synchrotron radiation. This has the usual harmonic structure. In an approximate evaluation of this radiation from a gyrating sheet we find that two effects contribute equally to the amplitude of the 2nd harmonic emission: the oscillation of the retarded time and the "beaming" effect due to the term $(1 - v_x/c)^{-1}$. One must therefore resist the temptation to neglect the latter term in the numerical solution. The approximate intensity of incoherent emission at the 1st and 2nd harmonics from sheets with a Maxwellian velocity distribution is evaluated for later comparison with measured emission.

In thermal equilibrium the one dimensional radiation fields have a uniform energy density spectrum $dU = \frac{2\theta}{c}\, df$. We also examined the thermal radiation in the numerical model which uses a space-time grid. We find that the energy density spectrum is the same as in the continuum for all wavelengths (those $> 2\Delta x$) and frequencies (those $< 1/(2\Delta t)$) which can be represented on the space-time grid. This upper limit on the frequency is well above any to which the plasma can respond.

The system of equations for sheets and fields is solved numerically in a weakly relativistic approximation. The sheet motion is considered nonrelativistic but the retarded fields are fully relativistic in order that the harmonic radiation be accurate, as discussed above. Normally radiation leaving the slab is lost. The sheets were started with a Maxwellian velocity distribution and the fields were zero.

The average change in $\underline{v}$ during a time τ is measured for different

initial $|\underline{v}|$. This change consists of a rotation at very nearly the cyclotron frequency and a decay in magnitude which is believed due primarily to diffusion of gyration phase among the sheets (the decay is too fast to be radiation drag).

We begin the discussion of the frequency spectrum of the Poynting flux of emitted radiation by setting up an unusually clean formulation of the statistical problem. This formulation readily allows discussion of the meaning and reliability of various measurements made on a finite subset of the ensemble over a finite time. We use a common estimator for the spectrum, calculated with the aid of the fast Fourier transform and employing the Parzen spectral window. The Poynting spectrum can be measured inside as well as outside the plasma slab.

Spectrum measurements are presented for two cases having different ω_c. In the first ($\omega_h=2\omega_c$) emission is strongest at ω_h with weak peaks at $3\omega_c$ and $4\omega_c$. The total emission power is only about 4% of what would be expected from incoherent cyclotron radiation, although no part of the spectrum is at the black-body level.

In the second case ($\omega_p=\omega_c$) the principal change in the spectrum is a strong peak at $2\omega_c$ which accounts for most of the emission power. This peak is about what would be expected from incoherent synchrotron radiation and would be slightly higher if not for reabsorption. It was found that the effect of the radiation fields on the sheet motion is such as to reduce the emission at ω_h, but not at $2\omega_c$, to well below the black-body limit.

In both cases there is evidence that no spectral component of the radiation originates in a localized region of the slab, such as the edge.

The spectra suffer from a broadening of their features probably due to there being too few sheets per Debye length.

VII. Future Work

In all this work the slab has been near thermal equilibrium. Thus the whole rich field of non-thermal and unstable plasma effects remains untouched, though not for long. Even without the radiation field, the loss-cone velocity distribution yields a natural elaboration of the two-stream instability work. With the radiation field one could look for the greatly enhanced high-harmonic emission sometimes seen in laboratory plasmas.

Before more work is done, the simulation code needs rewriting. In particular, the accurate handling of the discontinuous electrostatic field of thin sheets should be abandoned, probably in favor of the cloud-in-cell method as refined by Birdsall (19). This greatly reduces high frequency and short wavelength noise and allows larger time steps in the integration of the sheet motion. It will probably be necessary to keep the time steps for the radiation field small.

In future runs with such a code, one would use a much larger number of sheets per Debye cloud. Amongst other things, this result in lower collisional dissipation and may thereby allow closer and more realistic examination of the radiation spectra.

Phenomena involving relativistic effects, such as the shift of the cyclotron frequency, pose no difficulty. The radiation fields are already relativistically correct; the sheet equations need only the radiation B_z and the relativistic mass corrections. Unfortunately our simple and accurate one-dimensional method does not generalize to more dimensions. One can foresee difficulties in integrating the time dependent Maxwell equations. The delta-function nature of J_y can give trouble with finite-difference schemes, especially since the force on a particle due to its own field must be especially accurate in order to avoid gross self-acceleration errors. Again

smearing out the charge into a cloud is promising. Because it is so large, the longitudinal electric field must be quite accurate. Such accuracy may not be convenient or possible using the $\nabla \times \underline{B}$ equation to advance the whole $\underline{E}$ field in time. Instead it might be advisable to separate $\underline{E}$ into its longitudinal and transverse components, and solve accurately for the longitudinal component at each time step as in present codes. For the transverse $\underline{E}$ and $\underline{B}$ fields one might profitably solve for the potential $\underline{A}$ in the Coulomb guage.

Much theoretical analysis is lacking, particularly for those matters usually answered by dressed test-particle calculations: excitation by particles of longitudinal and transverse fields, and velocity space diffusion and drag. Also interesting are the fairly simple yet exact integral equations for the fields in a Vlasov gas having an arbitrary density profile, which are attractive for numerical solution.

Authors of computer simulation theses usually offer a paean to the computers of the future. Since there were usually much more powerful computers available elsewhere, the paean should properly have been directed to the computers in the author's personal future. For most of us progress in simulation is retarded more by lack of access to computers than by the state of the art in computer hardware. The work presented here was done on two antiquated machines without inconveniencing the many other users. Although the model code can be made faster, a thorough study of this model will require an order of magnitude more computation. This author also looks forward to the day when computation cost vs. knowledge gained will be judged on the same scale as for experimental programs.

APPENDIX I

The Dielectric Tensor With Dissipation

Here we explore the change in the dielectric tensor and dispersion relation when the simple relaxation term $-\nu f_1$ is added to the perturbed Vlasov equation. The only change in the Fourier-analyzed equations is that ω in the Vlasov equation is changed to $\omega + i\nu$ but ω in the Maxwell equations is unchanged. We denote by subscripts ν and 0 quantities derived with and without the term $-\nu f_1$.

In finding the conductivity $\underline{\underline{\sigma}}$, Faraday's law is used to eliminate the perturbed magnetic field $\underline{B}_1$ in favor of $\underline{E}_1$. However in our case the terms involving $\underline{B}_1$ are zero. Therefore $\underline{\underline{\sigma}}_\nu(k,\omega) = \underline{\underline{\sigma}}_0(k,\omega+i\nu)$.

In the Maxwell-Ampere law we replace $\frac{4\pi}{c}\underline{J}_1 - i\frac{\omega}{c}\underline{E}_1$ by $-i\frac{\omega}{c}\underline{\underline{K}}\cdot\underline{E}_1$, which defines $\underline{\underline{K}}$ as $\underline{\underline{I}} + \frac{4\pi i}{\omega}\underline{\underline{\sigma}}$. So in our case

$$\underline{\underline{K}}_\nu(k,\omega) = \underline{\underline{I}} + \frac{\omega+i\nu}{\omega}\left(\underline{\underline{K}}_0(k,\omega+i\nu) - \underline{\underline{I}}\right) \qquad \text{AI.1}$$

Let us see what this does to the electrostatic dispersion relation. If $K_0(k,\omega_0)=0$ (ω_0 is real for $\underline{k}$ real) and $K_\nu(k,\omega_0+\delta\omega)=0$ and ν is small enough,

$$\delta\omega = -i\nu\,\frac{\omega_0\frac{\partial K_0}{\partial\omega} - 1}{\omega_0\frac{\partial K_0}{\partial\omega}} \qquad \text{AI.2}$$

$$= -i\nu\,\frac{\text{Wave energy in particles}}{\text{Total wave energy}}$$

This last expression has a simple explanation. The relaxation term transfers particles from f_1 to the backround at a rate $-\nu f_1$, eliminating their contribution to the wave energy at a rate ν times the wave energy in the particles. From this physical argument one might conjecture eqn. AI.2 to be more general than for just the electrostatic waves, if the appropriate wave energies are used and $\nu\frac{\partial K}{\partial\omega} \ll K$.

When the wave energy in the particles is >0, the $-\nu f_1$ contribution to the time damping rate is always less than ν, approaching ν when most of the wave energy is in the particles.

Note that if $0<\omega_0\frac{\partial K}{\partial\omega_0}<1$, we have $\delta\omega_i > 0$ indicating growth. Now we have a loss of negative wave energy, i.e. a gain of wave energy. Since the total

wave energy is still >0, the wave is growing.

It is interesting to notice that the charge continuity equation in perturbed quantities is now

$$\frac{\partial \rho_1}{\partial t} + \nabla \cdot \underline{J}_1 = -\nu \rho_1 \qquad \begin{pmatrix} \rho_1 \\ \underline{J}_1 \end{pmatrix} = \sigma \int dv \begin{pmatrix} 1 \\ \underline{v} \end{pmatrix} f_1$$

so that the Poisson equation in perturbed quantities becomes

$$\frac{\partial}{\partial t}\left(\rho_1 - \frac{1}{4\pi} \nabla \cdot \underline{E}_1\right) = -\nu \rho_1$$

This is what one must use to derive the electrostatic dispersion relation after solving the Vlasov equation for ρ_1 instead of $\underline{J}_1$. The other Maxwell equations for perturbed quantities are unchanged. The physical explanation is that the relaxation term, in removing particles from f_1, destroys their contribution to $\underline{J}_1$ but not their contribution to $\underline{E}_1$.

APPENDIX II

Radiating Normal Modes of a Cold Slab

We have calculated the incoherent radiation from sheets moving independently of each other. The in-phase motion of N sheets radiates at a rate N times faster than the incoherent rate, if $kN/n_0 \ll 1$. The resulting radiation damping rate for in-phase motion can be quite comparable to the oscillation frequency. We therefore expect electrostatic standing wave oscillations in a thick slab to be strongly coupled to the radiation field outside.

In this connection it is interesting to consider the radiating normal modes of a cold system of sheets, i.e. we look for exponential time dependence of the fields and sheet velocities when the radiation field is the retarded solution for nonrelativistic motion, and the sheets do not cross. The governing equations are then

$$-\omega^2 Y_s = i\omega\omega_c X_s + i\omega\tau_r^{-1} \sum_{s'} Y_{s'} \exp\left(i\frac{\omega}{c}\Delta x\,|s-s'|\right)$$

$$-\omega^2 X_s = -\omega_b^2 X_s - i\omega\omega_c Y_s$$

with $\tau_r^{-1} = 2\pi\sigma^2/(mc)$. This yields

$$i\omega\tau_r \frac{\omega^2-\omega_i^2}{\omega^2-\omega_b^2} Y_s = \sum_{s'} Y_{s'} \exp\left(i\frac{\omega}{c}\Delta x\,|s-s'|\right) \qquad \text{AII.1}$$

If we write this system as a homogeneous matrix equation we can see a way to reduce the matrix to tridiagonal form. The rows in the tridiagonal matrix are formed from the corresponding rows in the original by multiplying the row by $-2\cos\Delta t$ and adding the rows immediately above and below. A similiar linear combination is made of the first and last pairs of rows to get the new first and last rows. The result is

$$\begin{pmatrix} A & -G & & & & \\ -G & B & -G & & & \\ & -G & B & -G & & \\ & & \ddots & \ddots & \ddots & \\ & & & -G & B & -G \\ & & & & -G & A \end{pmatrix} Y = 0 \qquad \text{AII.2}$$

in which $G = \omega \tau_r \frac{\omega^2 - \omega_h^2}{\omega^2 - \omega_p^2}$ $\qquad B = 2(\sin\omega\Delta t + G\cos\omega\Delta t)$

$$A = B - G\exp i\omega\Delta t$$

The physics behind the reduction and behind this form is as follows: Consider any three sheets moving in the combined fields generated by each other, the sheets to the left and the sheets to the right. From their equations of motion we eliminate the latter two fields. To eliminate two independent quantities we need three equations, which is why we consider three sheets and why we finish with a second order difference equation. The mathematical operation of elimination is exactly the same as the reduction performed above, which eliminated the other elements on a row corresponding to the left and right-going fields from the other sheets. At the outermost sheets there is only one field to eliminate (since there is no incoming radiation) so we consider only two sheets.

The solutions to this system are sinusoidal symmetric and antisymmetric. For 2N+1 sheets numbered -N to N we get the dispersion relation

$$G\cos k\Delta x = \sin\omega\Delta t + G\cos\omega\Delta t$$

or $$\left(\frac{c\sin(k\Delta x/2)}{\Delta x/2}\right)^2 = \left(\frac{\sin(\omega\Delta t/2)}{\Delta t/2}\right)^2 - \omega_p^2 \frac{\omega^2-\omega_p^2}{\omega^2-\omega_h^2}\left(\frac{\sin\omega\Delta t}{\omega\Delta t}\right)$$

and the boundary conditions

$$A\cos kN\Delta x = G\cos k(N-1)\Delta x \qquad \text{for } Y_s = \cos k\Delta x\, s,$$

$$A\sin kN\Delta x = G\sin k(N-1)\Delta x \qquad \text{for } Y_s = \sin k\Delta x\, s$$

As $k\Delta x \to 0$ the difference equations become

$$-c^2 Y''(x) = \frac{(\omega^2-\omega_+^2)(\omega^2-\omega_-^2)}{\omega^2-\omega_h^2} Y(x) \qquad \text{AII.3}$$

and the boundary conditions are

$$Y'(-R) = -i\frac{\omega}{c} Y(-R)$$
$$Y'(R) = i\frac{\omega}{c} Y(R) \qquad \text{AII.4}$$

where 2R is the thickness of the slab. In this limit eqn. AII.1 becomes the simple integral equation

$$2i\omega Y(x) = \frac{\omega_p^2}{c}\frac{\omega^2-\omega_p^2}{\omega^2-\omega_h^2}\int_{-R}^{R} dx' Y(x')\exp\left(i\frac{\omega}{c}|x-x'|\right) \qquad \text{AII.5}$$

which is of course equivalent to the dispersion relation and boundary

conditions.

For simplicity let us look at the case $\omega_c=0$. The dispersion relation is then $c^2k^2=\omega^2-\omega_p^2$. Putting the expression for ω from the boundary conditions into this givies after rearranging

$$i\frac{ck}{\omega_p} = \pm\begin{Bmatrix}\cos kR\\ \sin kR\end{Bmatrix} \quad \text{for} \quad Y=\begin{Bmatrix}\cos kx\\ \sin kx\end{Bmatrix} \qquad \text{AII.6}$$

The solutions of this equation are grouped symmetrically in the 4 quadrants of the complex k plane -if k is a solution then so are -k, k^*, and $-k^*$. If we look for a symmetric mode with $kR \ll 1$ we find $k\approx i\omega_p/c$, $\omega\approx -i\omega_p^2R/c$. This is the mode in which the sheets move together coupled to radiation with spatial scale $\gg$R. We might well expect this to be the most strongly radiation damped mode, but this is not so. If we rewrite the equation as

$$\cosh ikR = \pm\frac{c\,ik}{\omega_p}$$

and look for solutions along the imaginary k axis we can see, by graphing both sides, that for R small enough ($\omega_pR/c\lesssim .66$) there are two solutions, the smallest being this one. The other is more strongly damped than this, and the damping increases as $R\to 0$. What is happening physically is this: in this mode ω_iR/c is so large that a sheet is slowed by the retarded fields from other sheets when they were moving much more rapidly than now. Thus the damping is enhanced. The thinner the slab, the faster must be the damping rate to make this work. This works better for the sheets on the sides than in the middle where they are closer to the rest of the sheets. Since the velocity exponential decay rate is the same for all, this means the sheets in the middle have lower velocities. This is the meaning of the large imaginary k.

As ω_pR/c is increased toward about .66 the two imaginary roots come together, and above .66 ($\omega/\omega_p\approx 1.5i$) move away from the imaginary axis symmetrically, approaching $\pm\pi/(2R)$. The other roots have $k_r=(n+\frac{1}{2})\frac{\pi}{R}$ for symmetric modes and $k_r=n\pi/R$ for antisymmetric modes. Linearizing eqn. AII.6 about these values gives $k_i\approx \pm ck_r/(\omega_pR)$.

Introduction of the static magnetic field couples the electrostatic oscillations of the slab to the radiation field. This creates a new branch in the solutions of the dispersion relation and a new set of modes.

In table AII.1 we have the first few modes for an example of a thin slab with $\omega_pR/c=\omega_cR/c=.3$. The upper branch modes are very little different from the case with no magnetic field. We can see the two pure imaginary

modes identified above; the other upper branch modes are electrostaic oscillations weakly coupled to the radiation field. They are characterized by $\omega \approx \omega_h$ and $RdY/dx \ll Y$.

Table AII.2 shows the lowest modes when $\omega_p R/c = \omega_c R/c = 2$, approximately the values for the model runs. The movement of the upper branch modes toward their asymptotic limit can be seen, and they are less strongly damped. As $\omega_p R/c$ is increased from its former small value the phase velocity of the lower branch modes first approaches c (where they are best coupled to the radiation field and hence most strongly damped) and then exceeds c (where $\omega \rightarrow \omega_-$). This process can be seen in 2 modes in this example.

As R increases further all the lower-order modes on both branches become weakly damped.

In conclusion, a cold plasma slab of the size used in the model simulation has all its upper branch modes strongly damped, while all but the first few lower branch modes are nearly electrostatic oscillations weakly coupled to the radiation field. The slab would seem to fit roughly the small slab description and is far from the large limit.

Table AII.1 Radiating normal modes of cold slab with $\omega_p R/c = \omega_c R/c = .3$, $\omega_h R/c = .434$, $\omega_- R/c = .185$, $\omega_+ R/c = .485$.

Upper branch:

Mode	Symmetry	kR	$-\omega R/c$
1a	s	.22i	.047i
1b	s	3.00i	2.98i
2	a	2.15+3.26i	2.16+3.25i
3	s	3.98+3.57i	3.99+3.57i
4	a	5.69+3.82i	5.70+3.82i
5	s	7.35+4.02i	7.36+4.02i
6	a	8.99+4.19i	8.99+4.19i

Lower branch:

Mode	Symmetry	kR	$-\omega R/c$
0	s	.48+.44i	.43+.023i
1	a	1.61+.26i	.42+.001i
2	s	3.15+.14i	.42+.00008i
3	a	4.71+.090i	.42+.00002i
4	s	6.28+.067i	.42+.00001i
5	a	7.85+.054i	.42+.00000i
6	s	9.42+.045i	.42+.00000i

Table AII.2 Radiating normal modes of cold slab with $\omega_p R/c = \omega_c R/c = 2$, $\omega_h R/c = 2.83$, $\omega_- R/c = 1.24$, $\omega_+ R/c = 3.24$.

Upper branch:

Mode	Symmetry	kR	$-\omega R/c$
1	s	1.42+.45i	3.32+.07i
2	a	2.78+.97i	3.62+.52i
3	s	4.35+1.49i	4.80+1.29i
4	a	5.97+1.81i	6.30+1.70i
5	s	7.58+2.05i	7.84+1.97i
6	a	9.18+2.24i	9.39+2.18i

Lower branch:

Mode	Symmetry	kR	$-\omega R/c$
0	s	.98+.76i	1.41+.38i
1	a	2.20+1.10i	2.22+.57i
2	s	3.40+.86i	2.57+.17i
3	a	4.80+.62i	2.69+.041i
4	s	6.32+.46i	2.75+.013i
5	a	7.87+.37i	2.78+.0049i
6	s	9.44+.31i	2.80+.0023i

APPENDIX III

Reflection and Transmission of Radiation

One would like to calculate theoretically what the spectrum of emitted radiation should be, and compare this with what is observed. Because of the difficulty with the test-sheet picture mentioned before, we turn first to Kirchoff's law. Part of the calculation of the reflection and transmission coefficients for the slab appears in the literature (20, 21, 22). These papers expand the linearized Vlasov equation in powers of $\frac{v_{es}}{\omega_c}\frac{\partial}{\partial x}$, going far enough to include the resonance at the 2nd harmonic of the cyclotron frequency. Bernstein and Weenink then go on to calculate the reflection and transmission coefficients for a slab like ours. Unfortunately the expression they use for the current in terms of the fields and their derivatives appears to suffer from cumulative algebraic indiscretions. One could substitute Pearson's result here and carry the calculation through again. Kuehl (23) has done this for a thin slab.

In these calculations for the uniform slab (21,23) all incident radiation is either reflected or transmitted. This is due to the lack of wave dissipation noted before. Kirchoff's law is thus not usable with their results. In the absence of wave-particle resonance, the usual dissipation mechanism in these calculations, one must presumably make use of collisions. Since no adequate kinetic theory exist for sheet plasmas in a magnetic field, we might resort to a simple relaxation term (Appendix I) in the linearized Vlasov equation. This calculation has not yet been carried through, although it would be interesting to do so.

For a slab with slowly varying density probably a better approach would be a WKBJ-type approximation which would not break down when wavelengths are small (collisionless absorption could occur at places in the plasma where $k \to \infty$. However the solutions of the exact dispersion relation indicate such singularities do not occur).

Let us consider how we might measure the reflection and transmission coefficients for the plasma model. Put another way, we want to measure the linear response of the model to radiation incident from one side. This must be done in the presence of the radiation emitted unbidden by the plasma. A method for decreasing the interference from this noise ("One man's noise is another man's signal." -W.B.Daniels) has been suggested by Y.W.Lee (24) and developed theoretically by N. R. Goodman (13). Incoherent radiation is sent

into the plasma from both sides. We estimate the crosscorrelations and cross-spectra between incoming and outgoing radiation, which estimate the reflective and transmissive impulse and frequency responses. We could also take the crosscorrelation of the input radiation and the radiation at many points inside the plasma and thus follow a pulse of radiation and its reflections as they move through the slab. The crossspectra would display the wave amplitude and phase for each frequency. This would be used to check the dispersion relation and studywave boundary conditions. Such a project requires a great deal of computation; fast Fourier (14) techniques are indicated.

There is a minor difficulty. Implicit in all this discussion has been the assumption that the system is time invariant. However for runs long enough to get good sampling variance the plasma changes appreciably through loss of energy through radiation. A resolution of this difficulty which fits neatly with the method of measuring the linear response may be to make the input radiation equal to the one- dimensional thermal (black-body) radiation over the range of frequencies the plasma is capable of responding to. Thus the plasma finds itself in a radiation field at the same temperature as itself, and so does not gain or lose energy on the average. One would have to check that the response was still sufficiently linear at such amplitudes.

In a trial of this idea, the impulse response of a single sheet was measured. Averaging over 140 p iods and 1250 time steps, the "noise" was about 10% of the amplitude of the peak response. The measured response was noise for negative times, and for positive times showed 6 oscillations before fading into the noise. The decay is due to radiation damping. The 2 natural frequencies of noncrossing motion, 0 and ω_h, show clearly. With a run of a few hundred periods the response of a many-sheet system should be accurately measurable.

REFERENCES

1 J. Dawson, Paper presented at the 1966 A. P. S. Division of Plasma Physics annual meeting, Boston Mass., Nov. 1966. Also Annual Report of the Plasma Physics Laboratory, Princeton University, 1966.

2 Bruce Langdon and John Dawson, Symposium on Computer Simulation of Plasma and Many-body Problems, Williamsburg Va., April 1967, (NASA SP153).

3 Ramy Shanny, John M. Dawson and John M. Greene, Phys. Fluids 10, 1281 (1967).

4 John Dawson, Phys. Fluids 5, 445 (1962).

5 O. C. Eldridge and M. Feix, Phys. Fluids 5, 1076 (1962).

6 O. Eldridge and M. Feix, Phys. Fluids 5, 1307 (1962).

7 T. H. Stix, The Theory of Plasma Waves, McGraw-Hill (1962).

8 I. B. Bernstein, Phys. Rev. 109, 10 (1958).

9 G. Bekefi, Radiation Processes in Plasmas, Wiley (1966).

10 D. E. Baldwin and G. Rowlands, Phys. Fluids 9, 2444 (1966).

11 N. G. Van Kampen, Physica 21, 949 (1955).

12 R. B. Blackman and J. W. Tukey, The Measurement of Power Spectra, Dover, New York (1959).

13 N. R. Goodman, Scientific Paper No. 10, Engineering Statistics Laboratory, New York University (1957).

14 Gentleman and Sande, Proceedings of the Fall Joint Computer Conference, Nov. 1966. This is a very readable review paper containing much information otherwise unpublished.

15 J. W. Tukey, An Introduction to the Frequency Analysis of Time Series, Mathematics 596 lecture notes (unpublished), Princeton University.

16 Langdon and Sande, IBM SHARE Program SDA3483.

17 G. Sande, fast Fourier transform programs, private communication, 1965.

18 J. W. Cooley, IBM SHARE Program SDA3465.

19 C.K. Birdsall and D. Fuss, UCRL-71068 (1968).

20 G. A. Pearson, Phys. Fluids 9, 2454 (1966).

21 I. B. Bernstein and M. P. H. Weenink, Euratom Symposium on Theoretical Plasma Physics, May 1966.

22 D. E. Baldwin, J. Plasma Phys. 1, part 3, 289 (1967).

23 H. H. Kuehl, Phys. Fluids 11, 456 (1968).

24 Y. W. Lee, Tech. Rep. No. 181, Research Laboratory of Electronics, M.I.T. (1950).

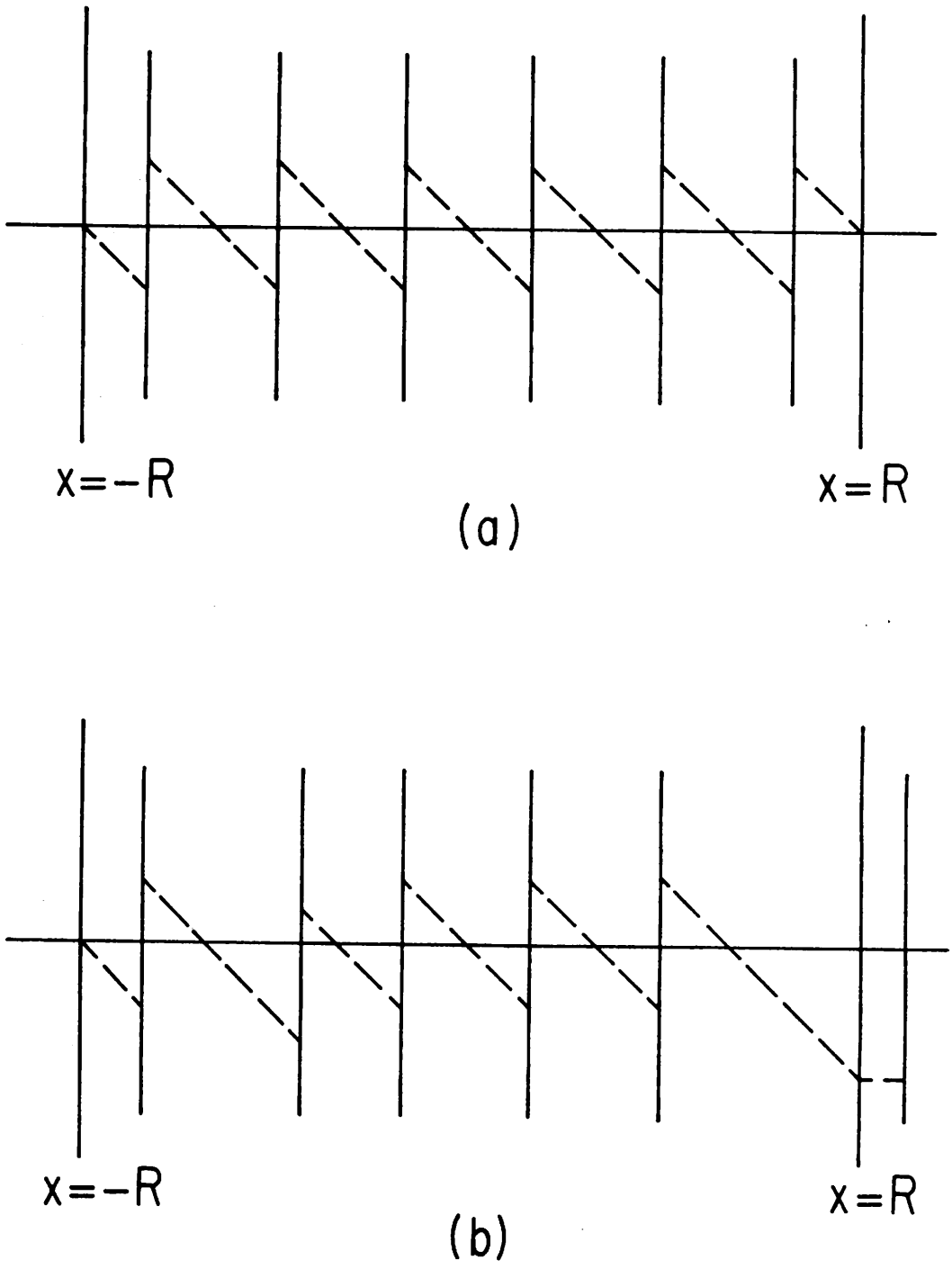

Fig. II.1 Electrostatic field (dashed line) in slab model, (a) with sheets in electrostatic equilibrium, and (b) with two sheets displaced. The field is zero outside the system.

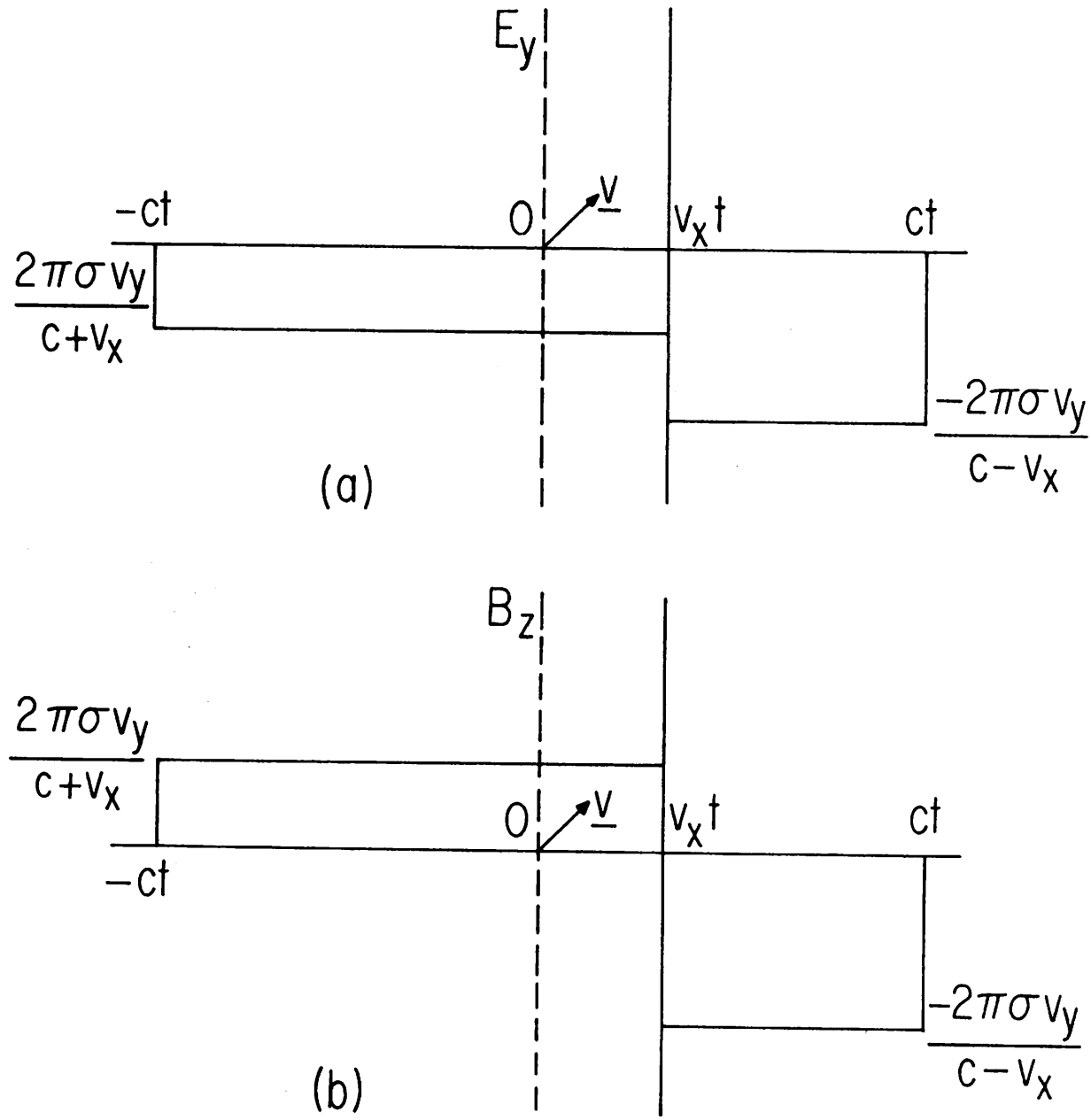

Fig. II. 2 The radiation fields E_y and B_z from a sheet at rest (x=0) for $t < 0$ and given a constant velocity for $t \geq 0$. Here $v_x/c=1/3$.

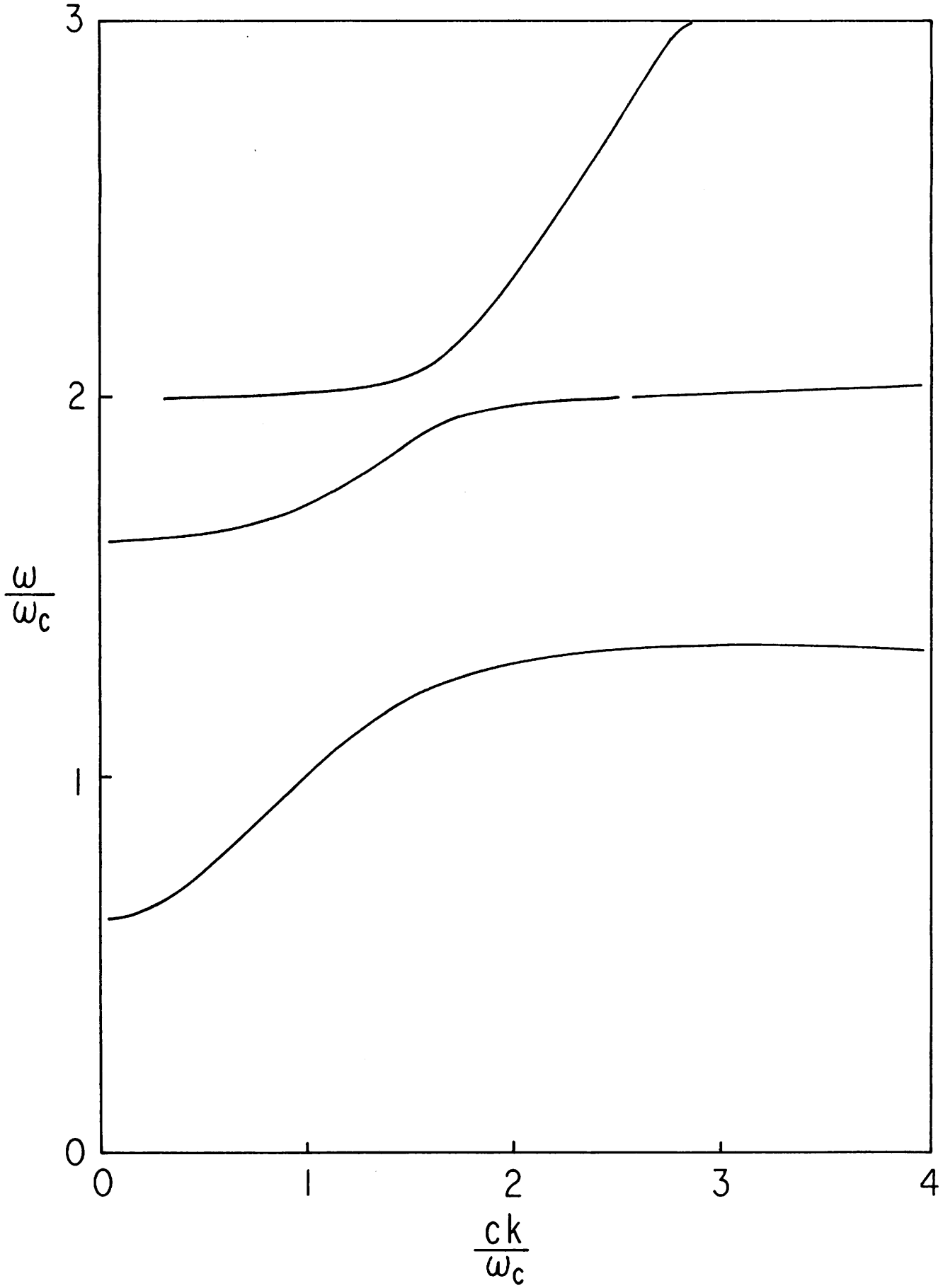

Fig. II. 3 Solutions of the electromagnetic dispersion relation for a Maxwellian velocity distribution. $\omega_p = \omega_c$, $v_{th} = .1\ c$

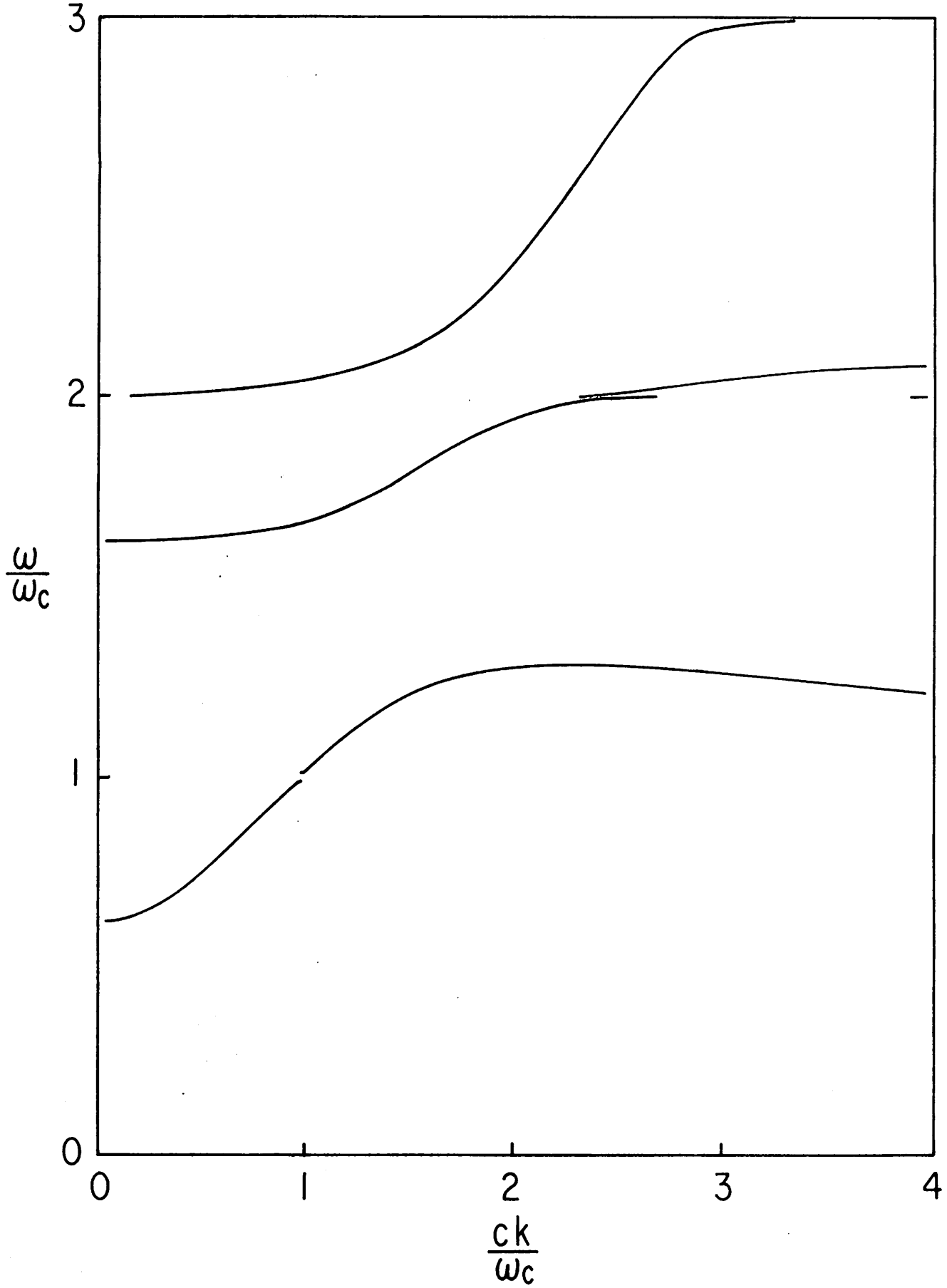

Fig. II. 4 Same as II. 3 except $v_{th} = .2\ c$

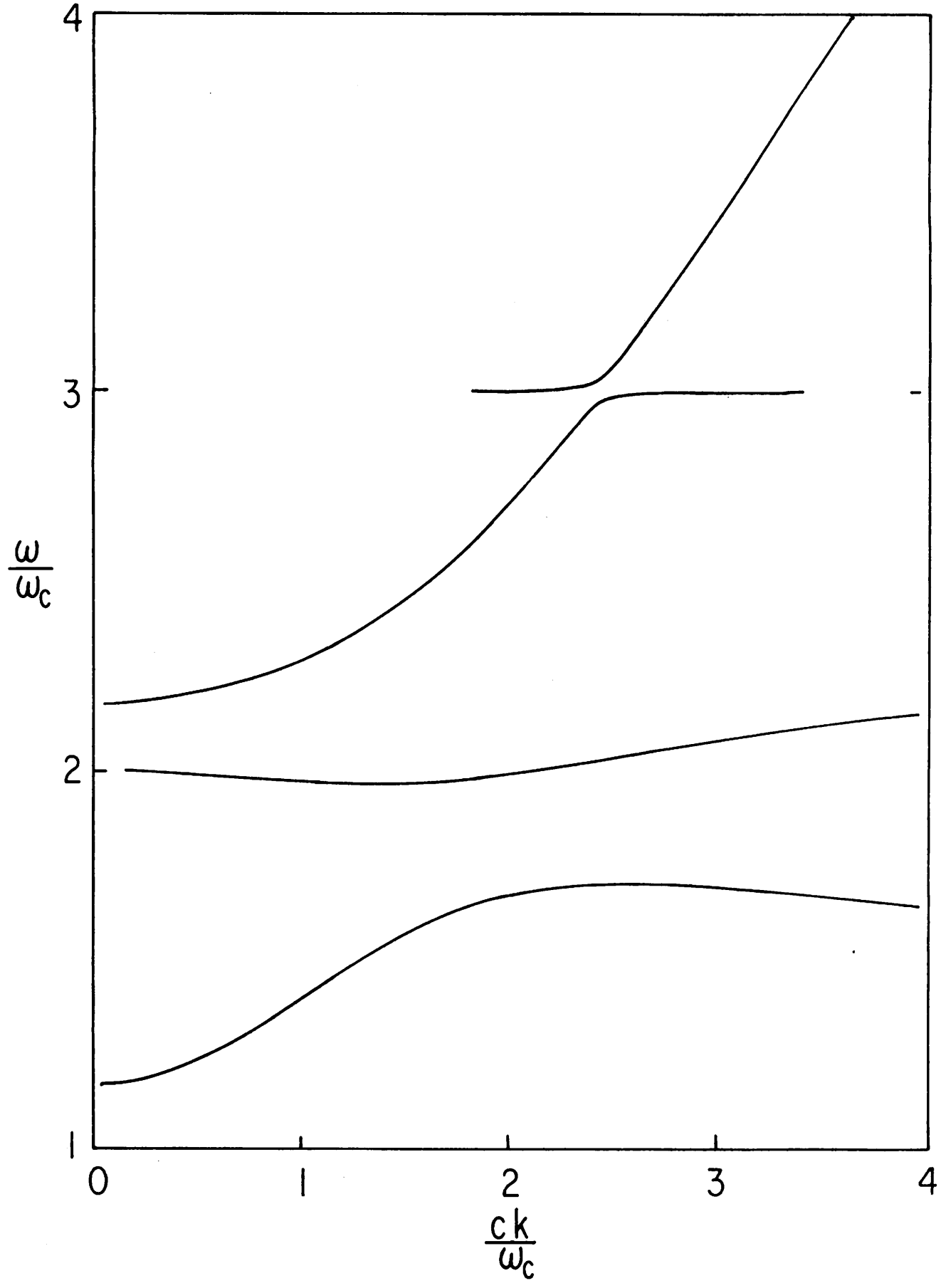

Fig. II. 5 Same as II. 3 except $\omega_p = 1.6\ \omega_c$

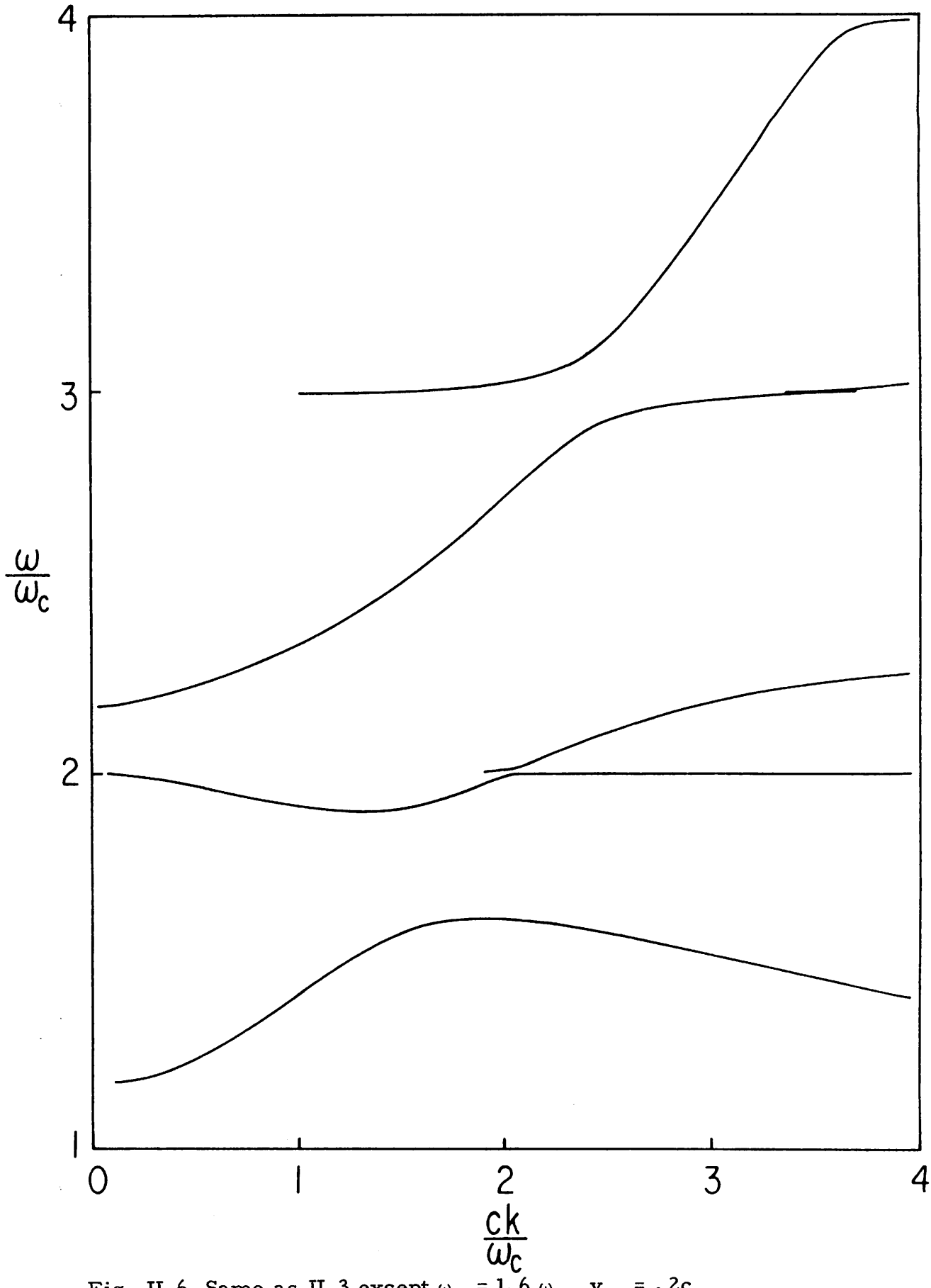

Fig. II. 6 Same as II. 3 except $\omega_p = 1.6\ \omega_c$, $v_{th} = .2c$

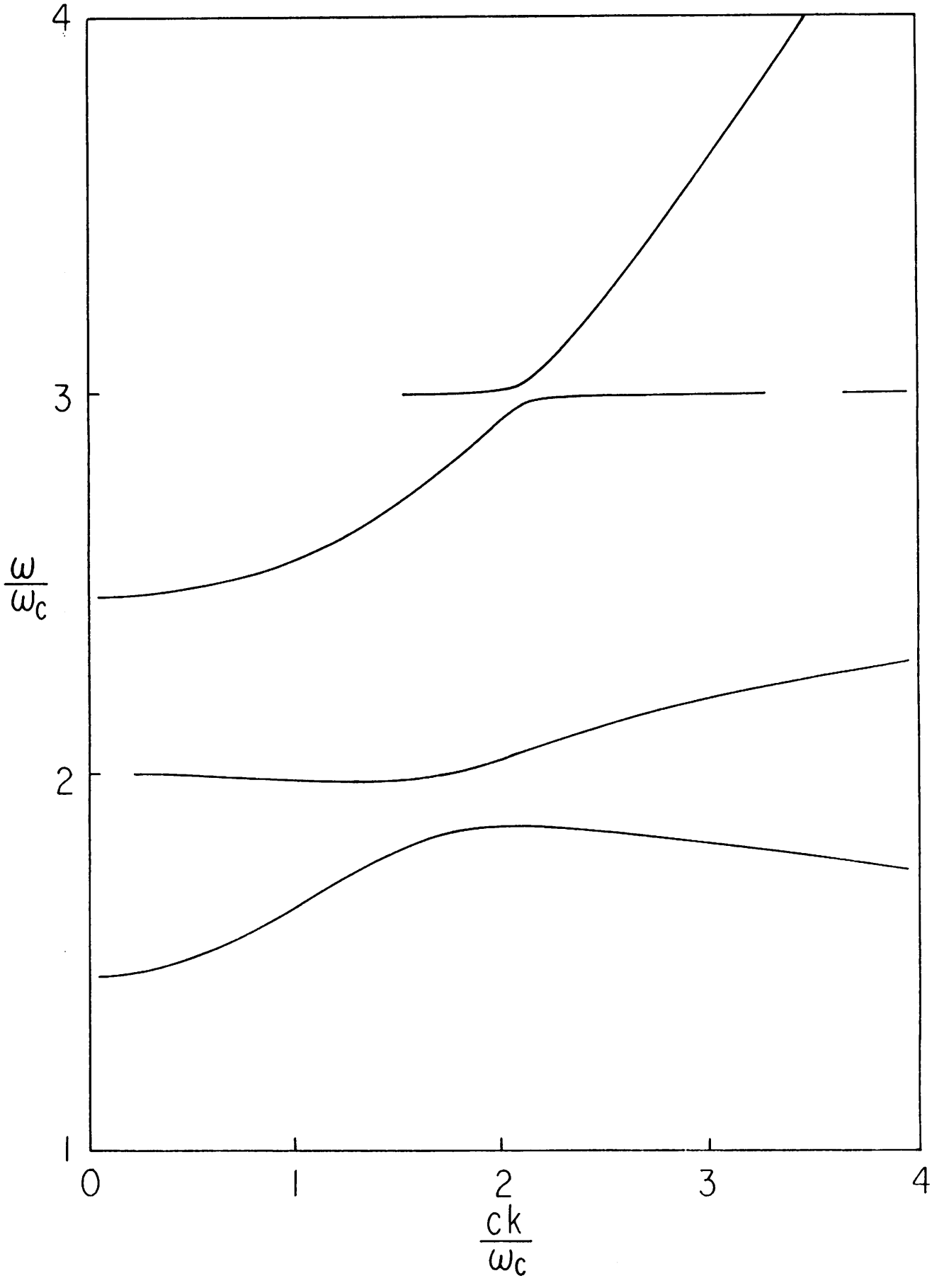

Fig. II. 7 Same as II. 3 except $\omega_p = 1.9\,\omega_c$.

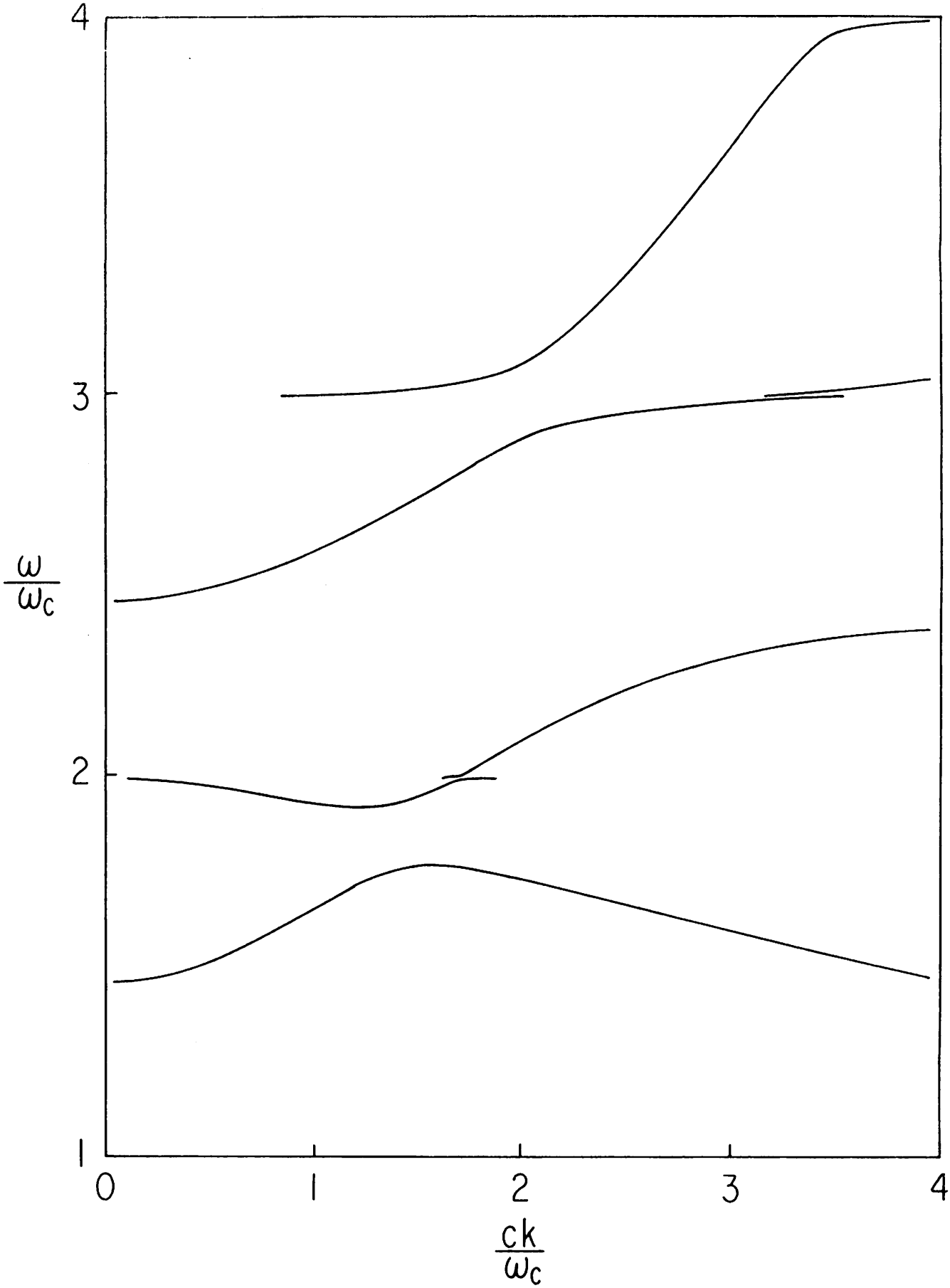

Fig. II. 8 Same as II. 3 except $\omega_p = 1.9\,\omega_c$, $v_{th} = .2c$.

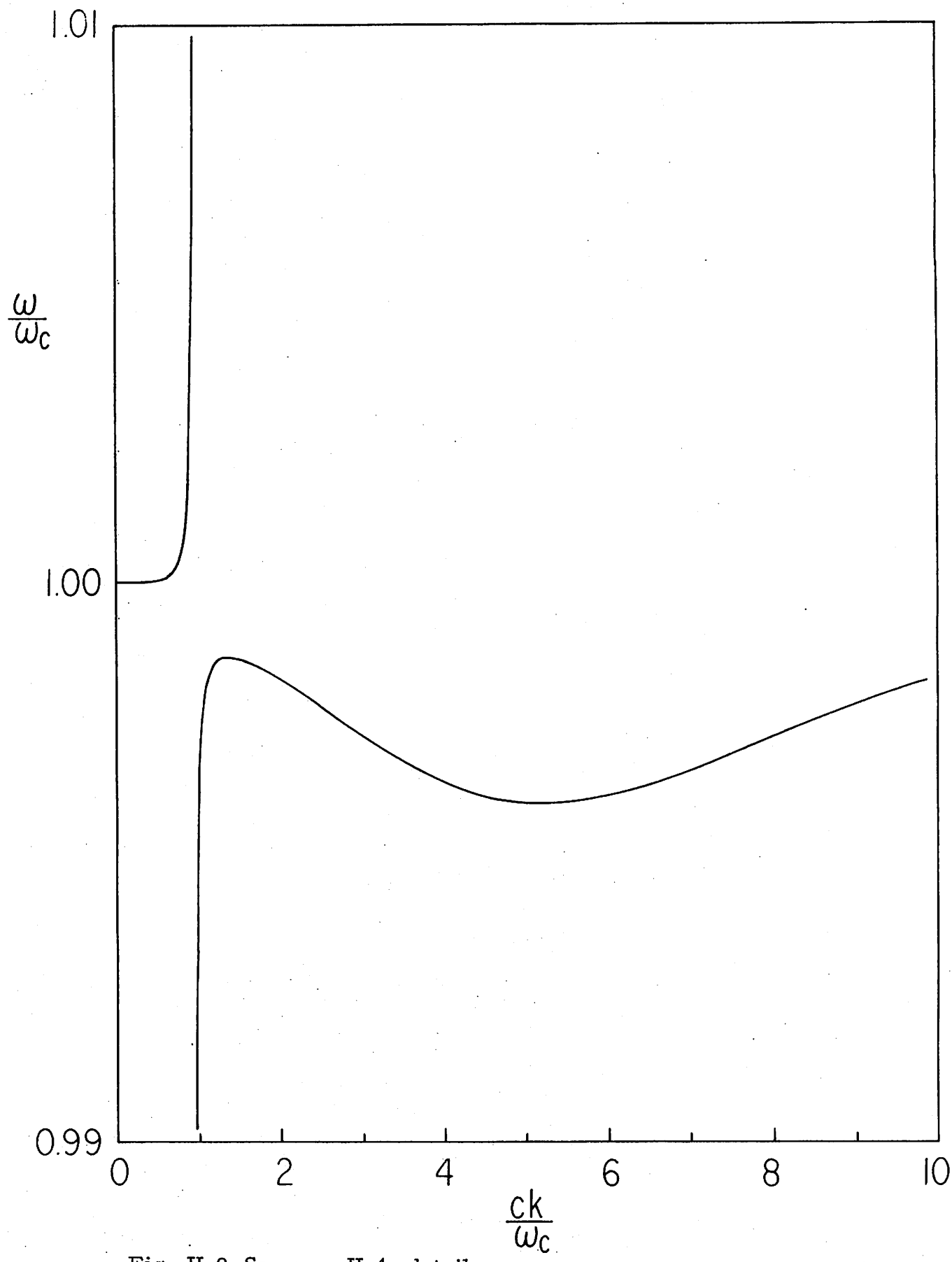

Fig. II. 9 Same as II. 4, detail near $\omega = \omega_c$.

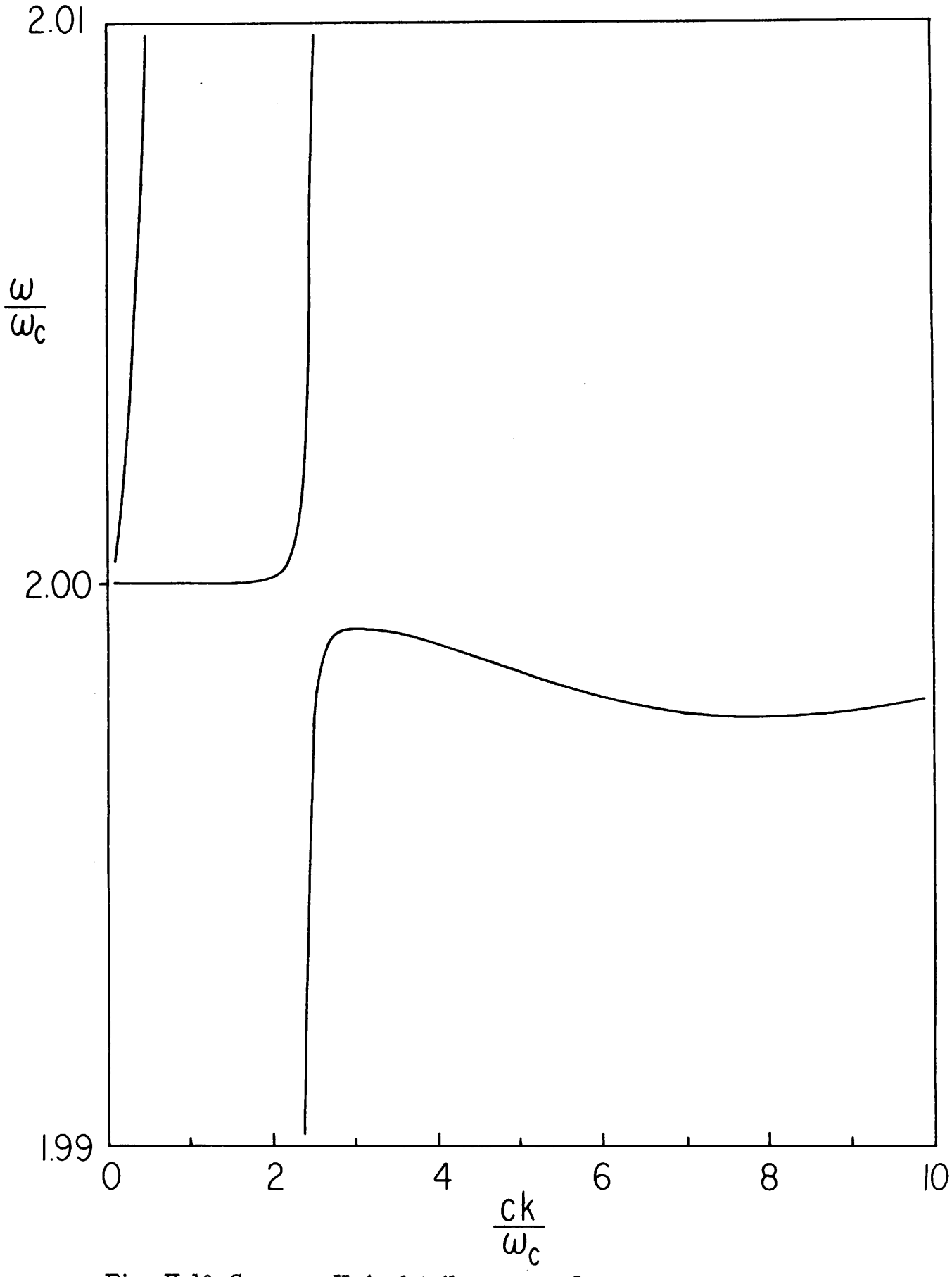

Fig. II.10 Same as II.4, detail near $\omega = 2\,\omega_c$

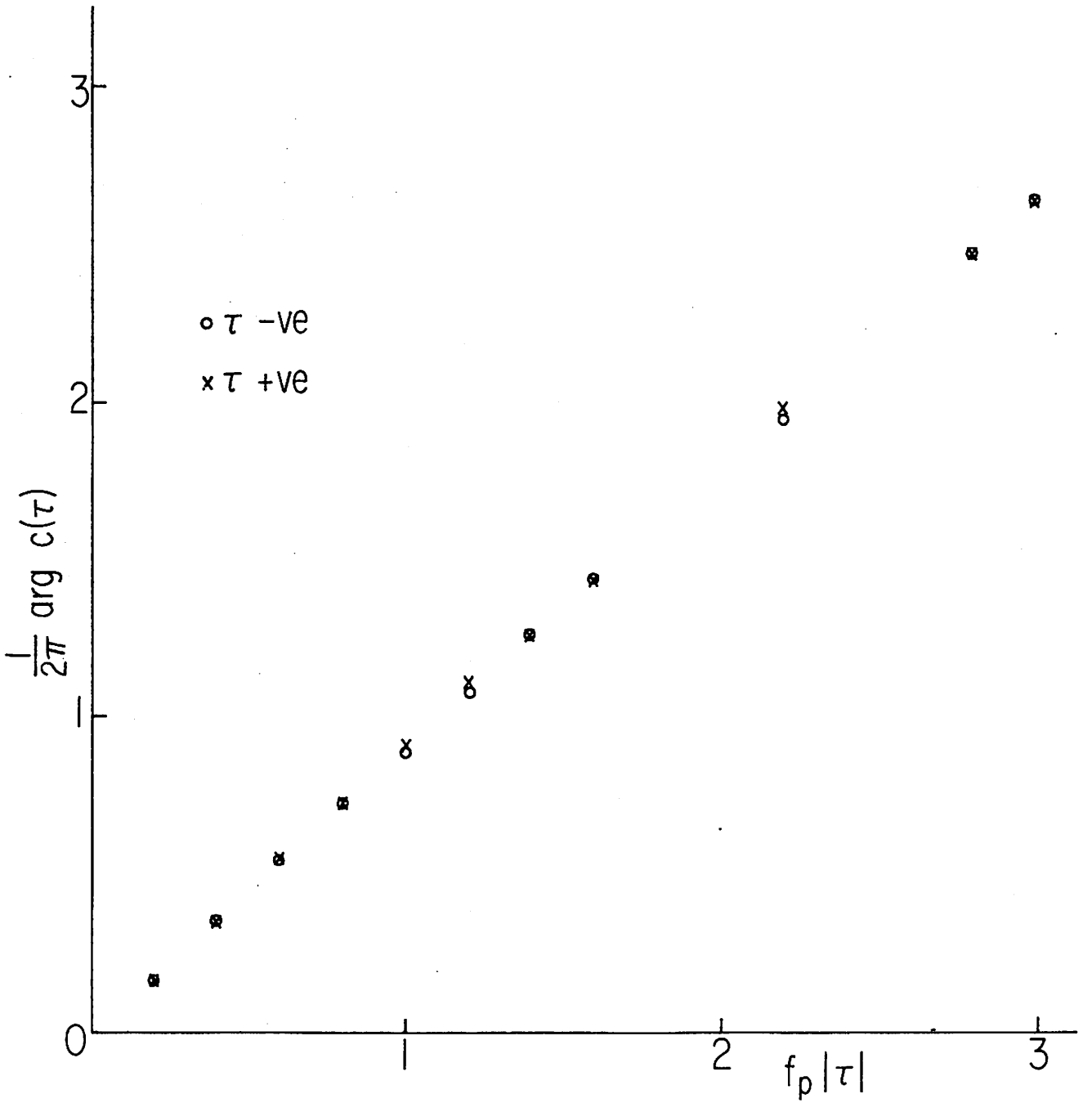

Fig. IV.1 Phase of $C(\tau)$ for $v_0 = .03$.

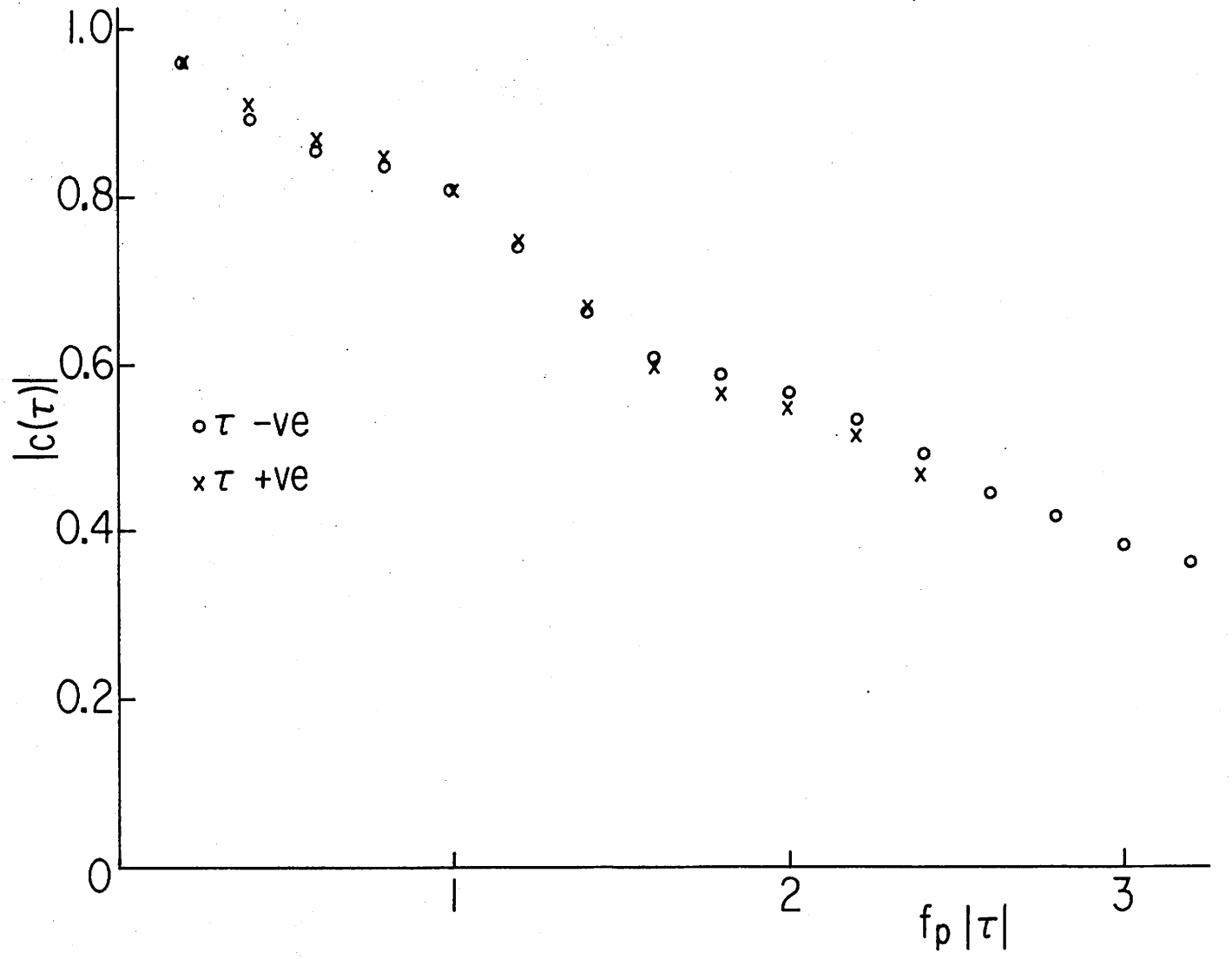

Fig. IV.2 Modulus of $C(\tau)$ for $v_0 = .03$.

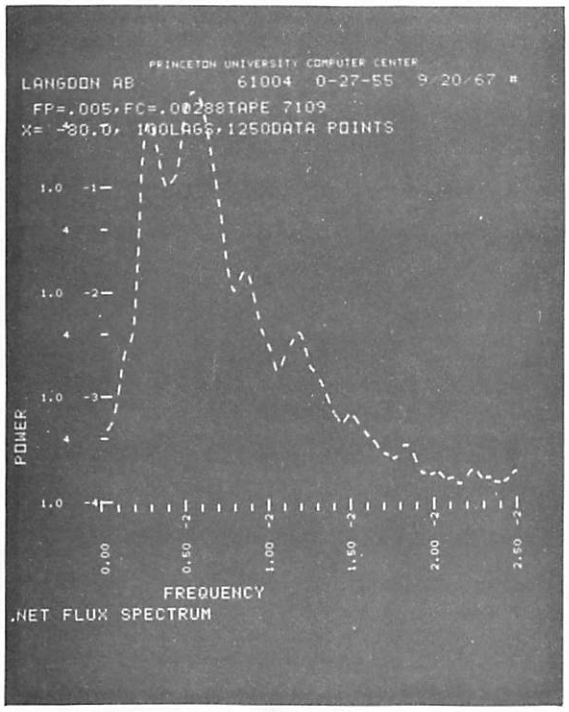

(a) X = - 80

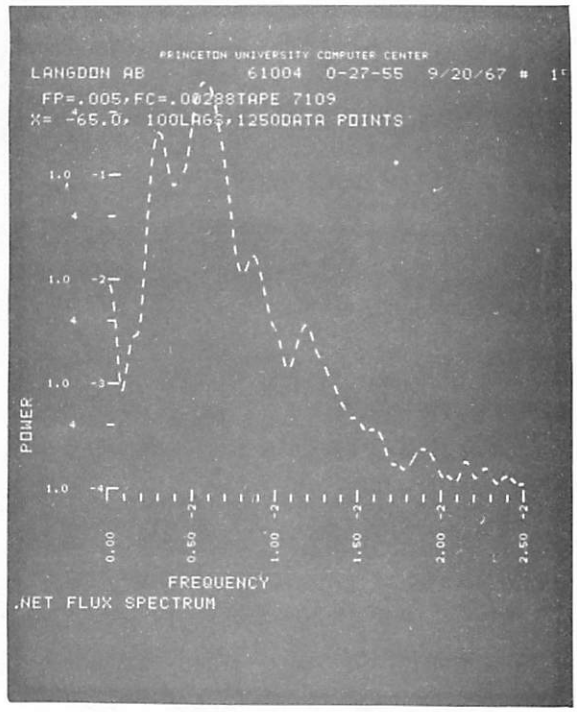

(b) X = - 65

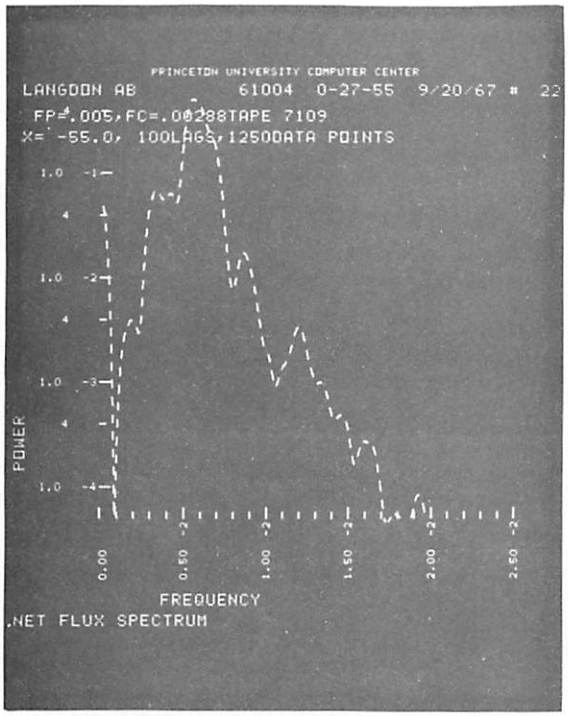

(c) X = - 55

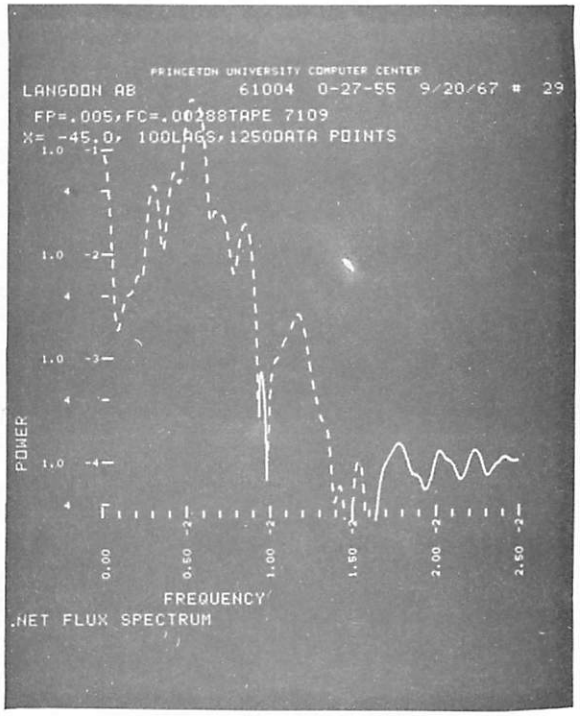

(d) X = - 45

(continued next page)

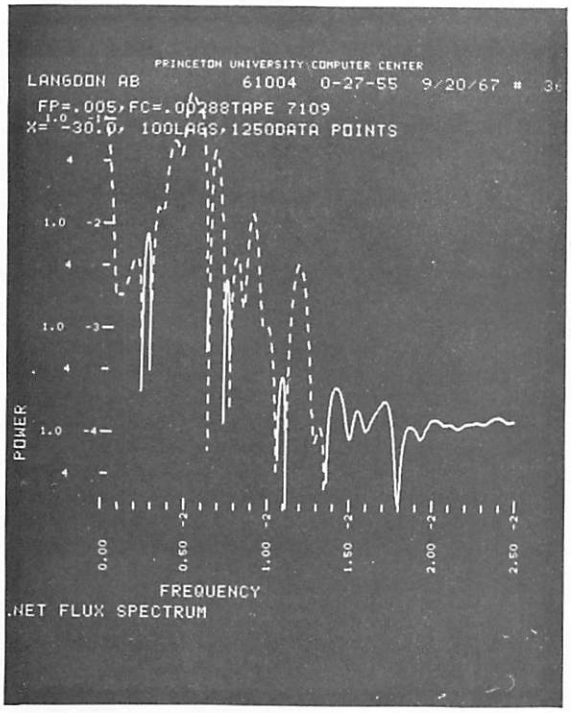

(e) X = - 30

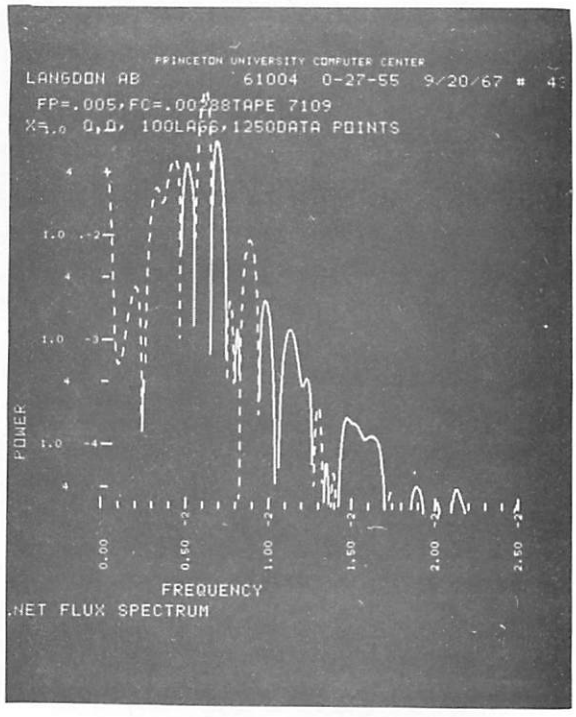

(f) X = 0

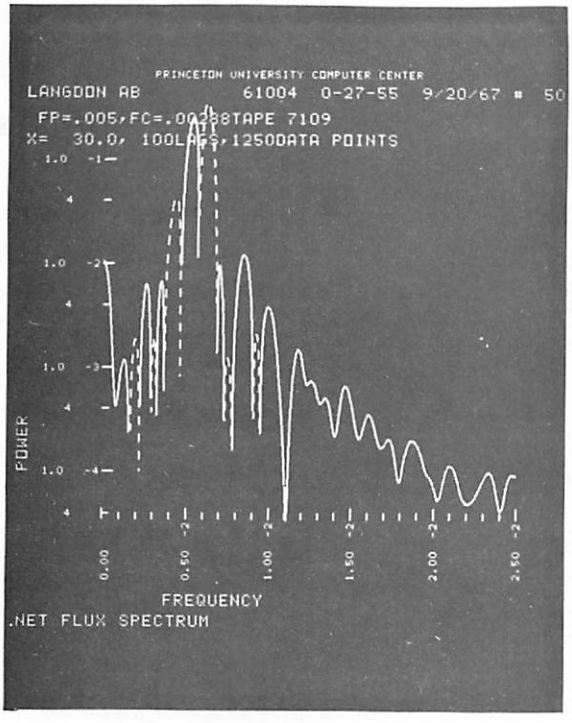

(g) X = 30

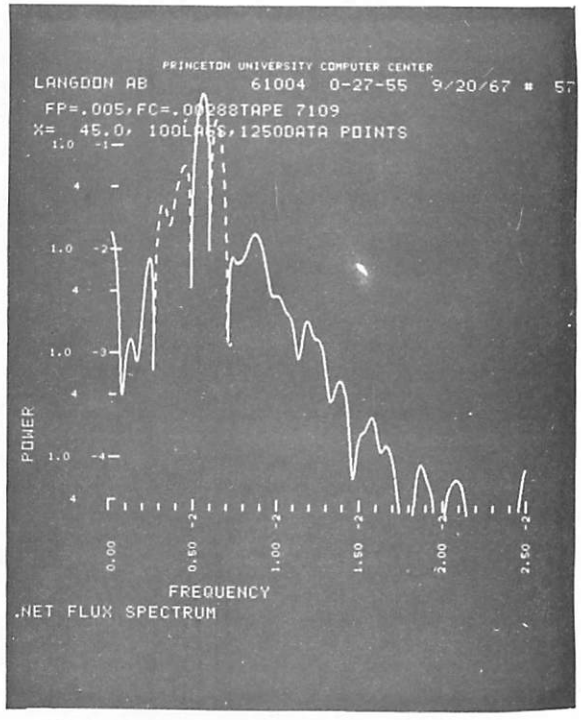

(h) X = 45

(continued next page)

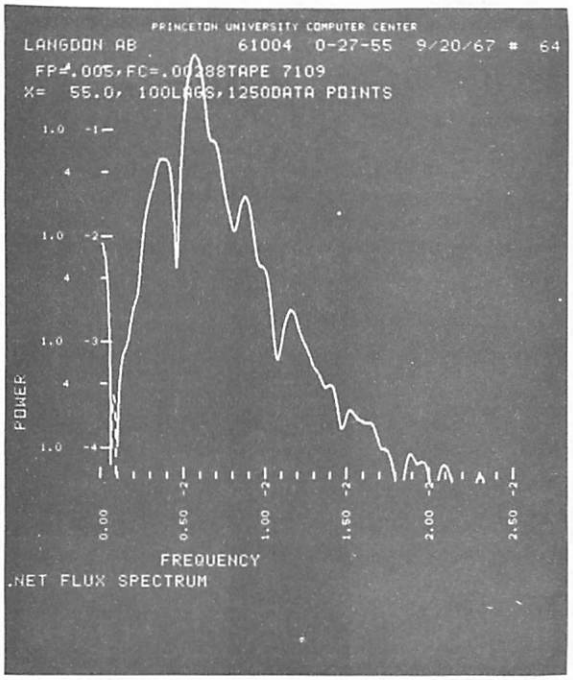

(i) X = 55

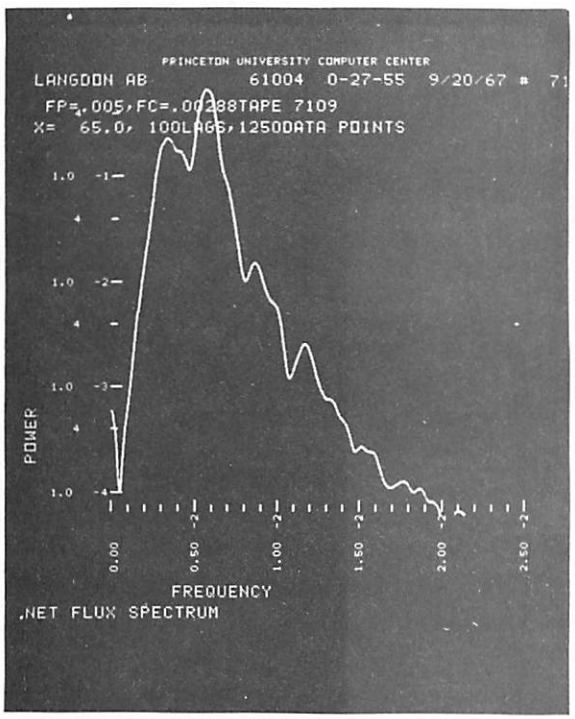

(j) X = 65

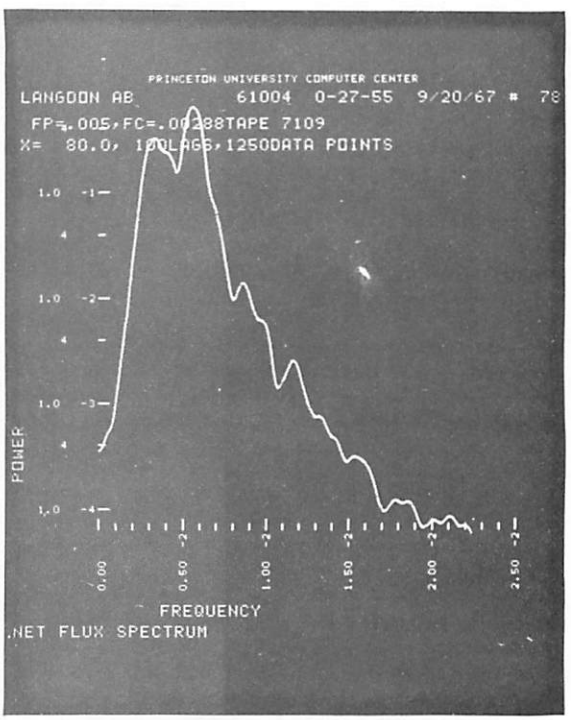

(k) X = 80

Fig. V. 1. Poynting flux spectrum

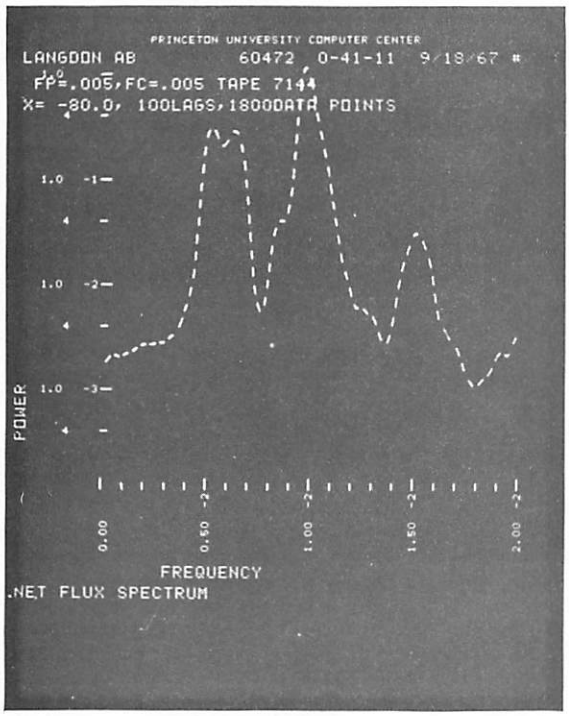

(a) X = - 80

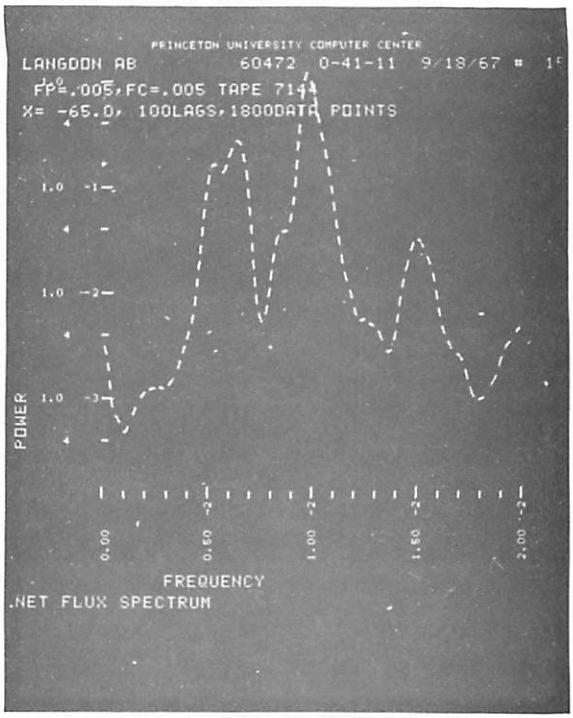

(b) X = - 65

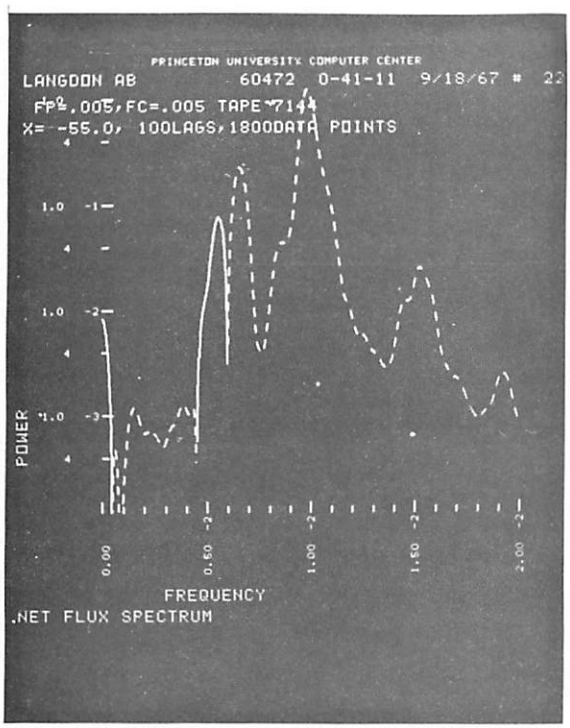

(c) X = - 55

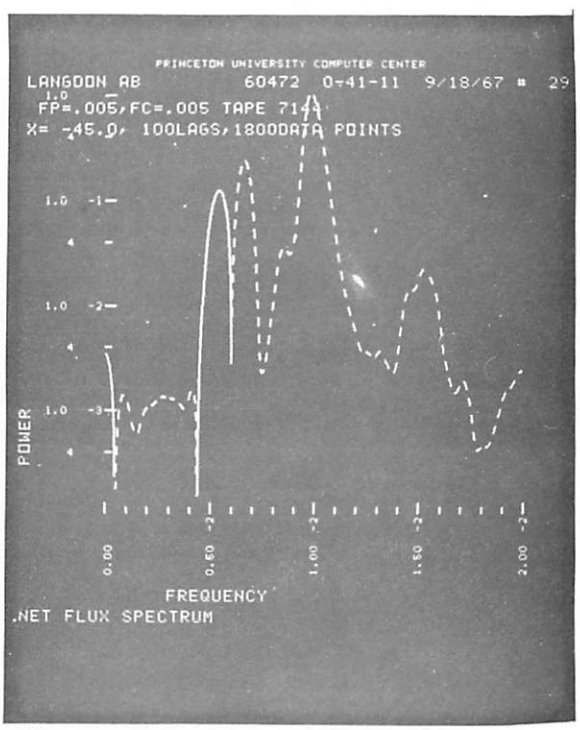

(d) X = - 45

(continued next page)

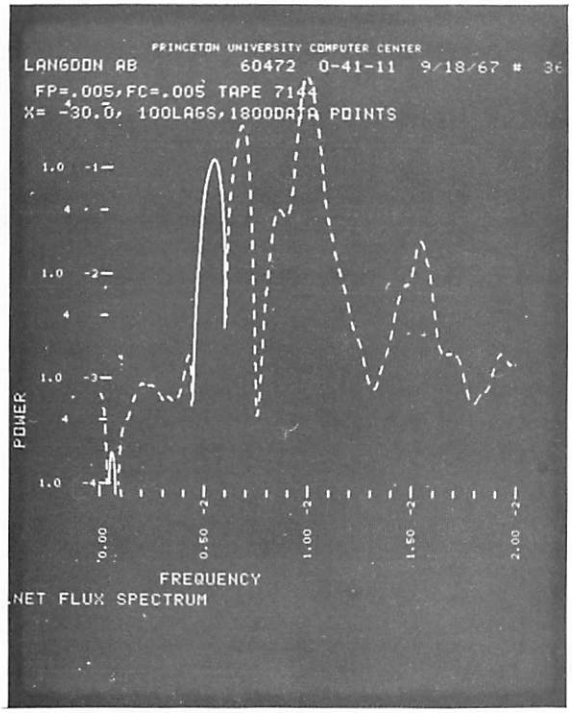

(e) X = - 30

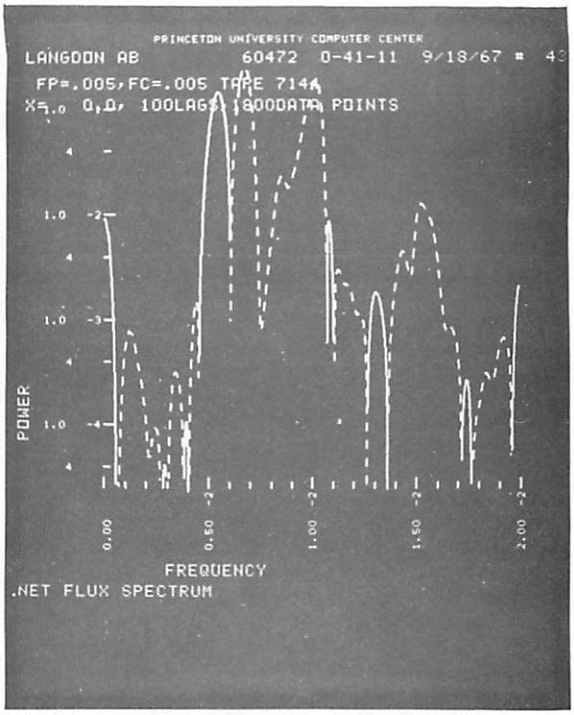

(f) X = 0

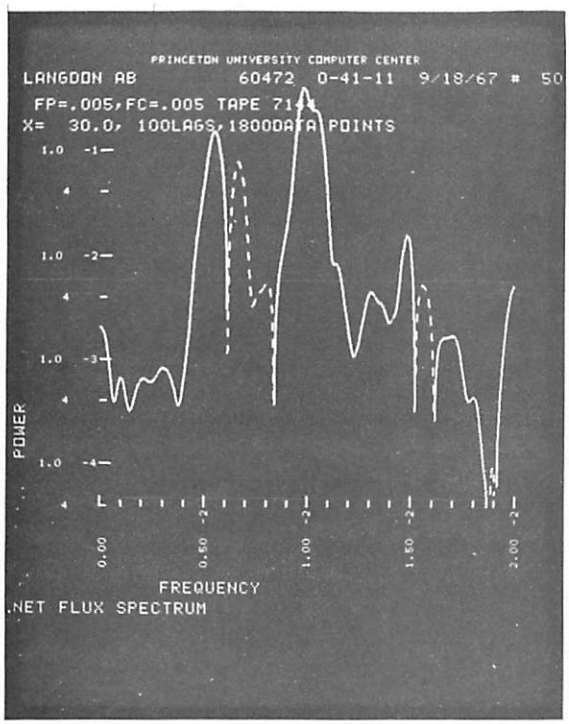

(g) X = 30

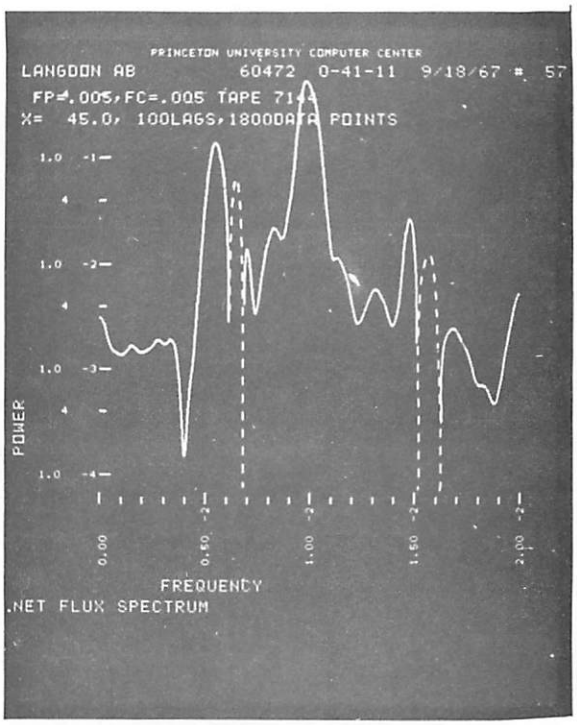

(h) X = 45

(continued next page)

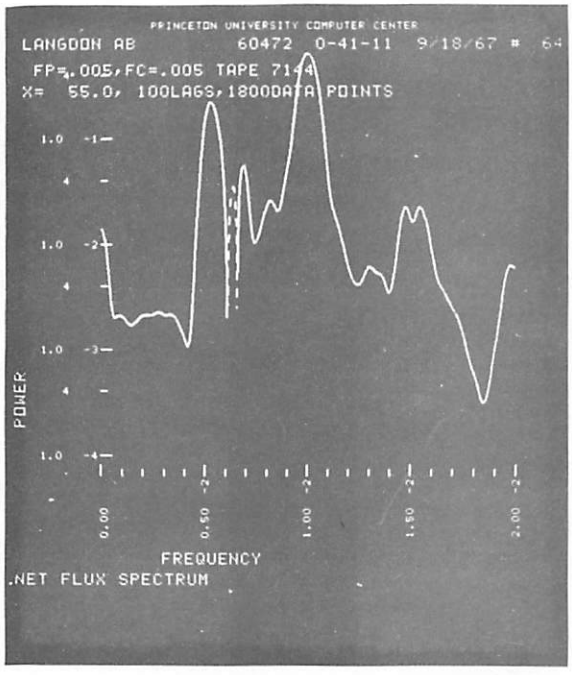

(i) X = 55

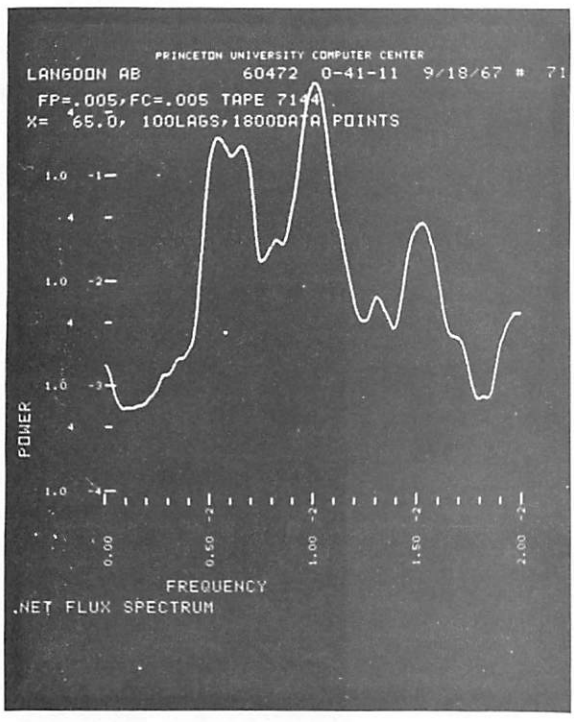

(j) X = 65

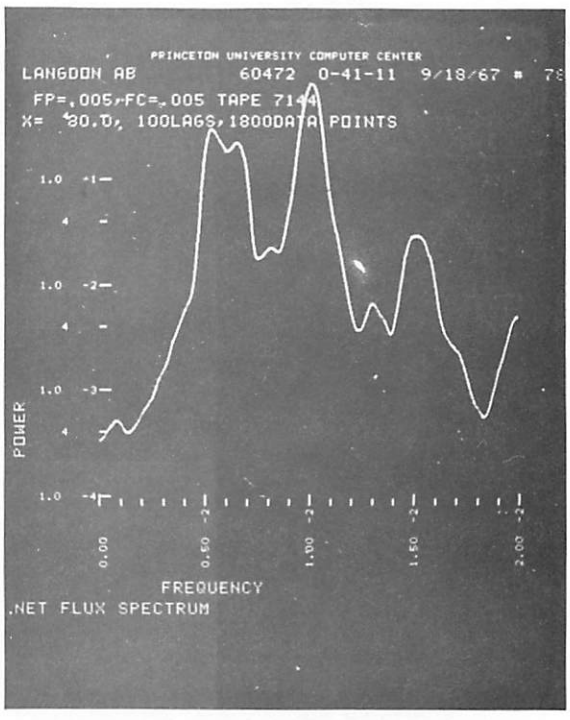

(k) X = 80

Fig. V. 2. Poynting flux spectrum

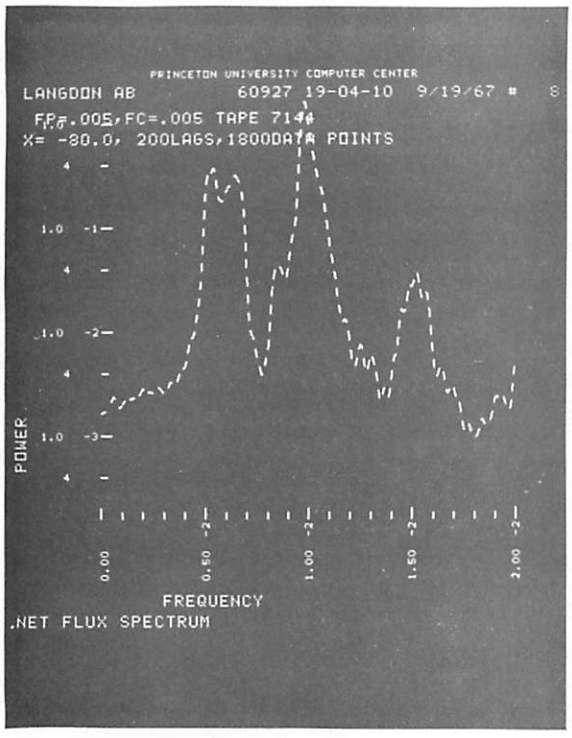

(a) X = - 80

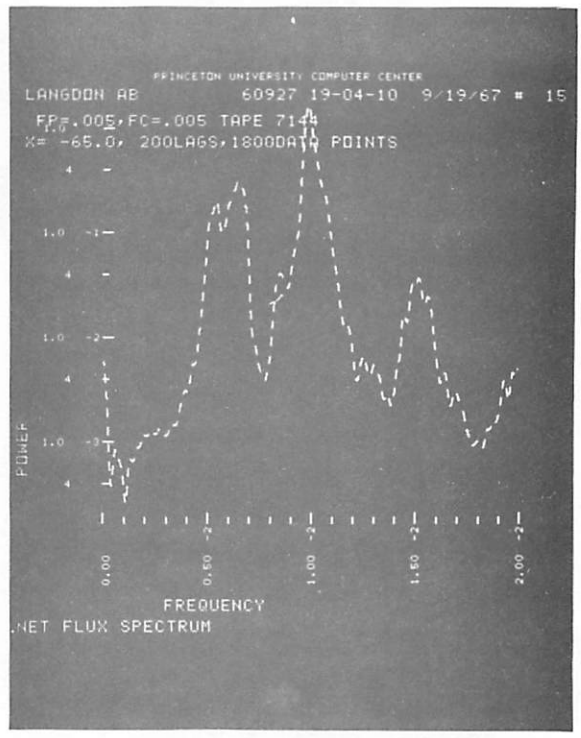

(b) X = - 65

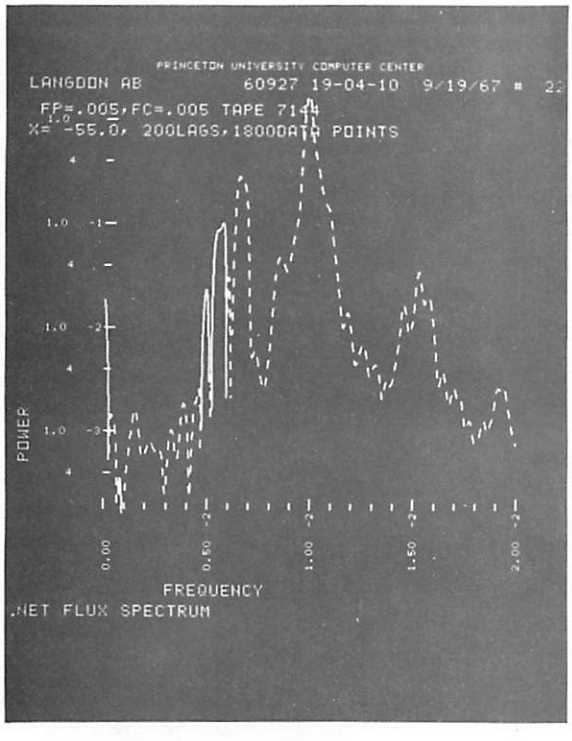

(c) X = - 55

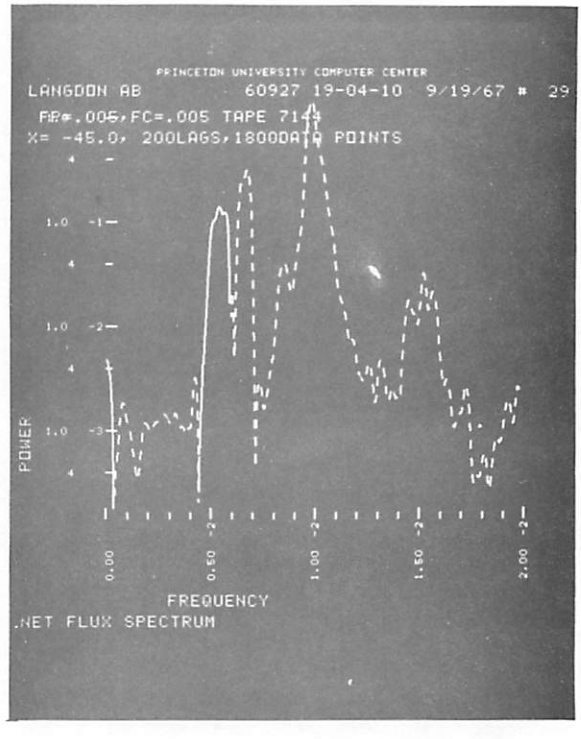

(d) X = - 45

(continued next page)

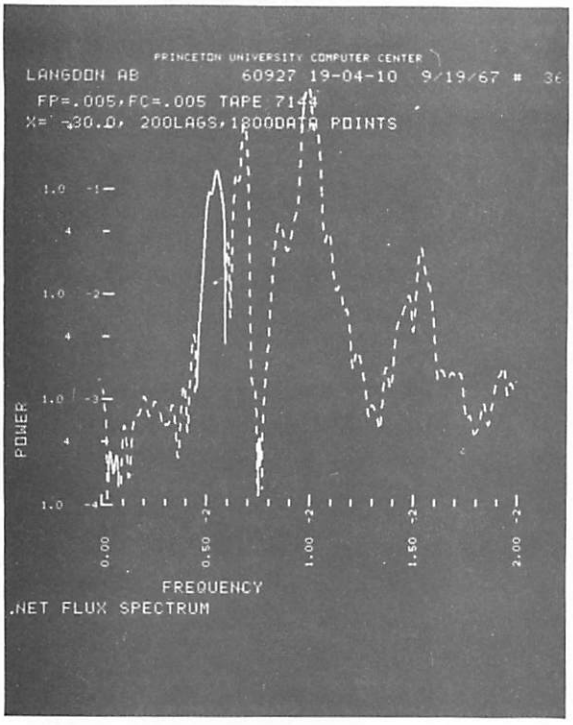

(e) X = - 30

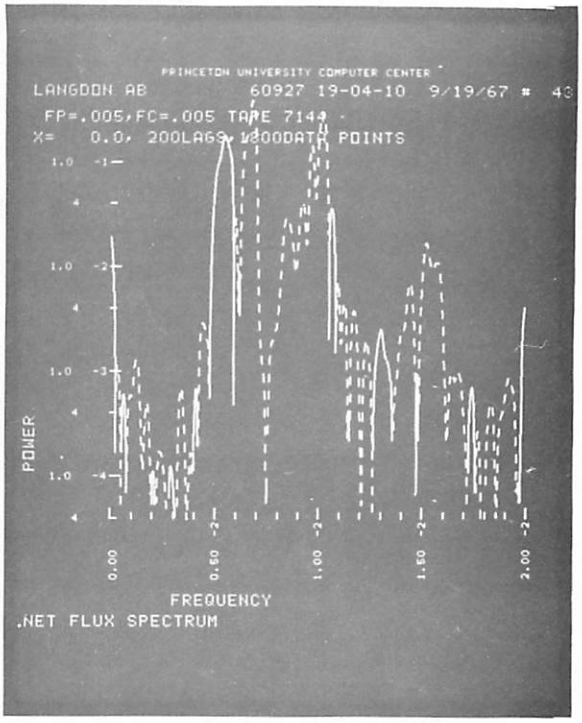

(f) X = 0

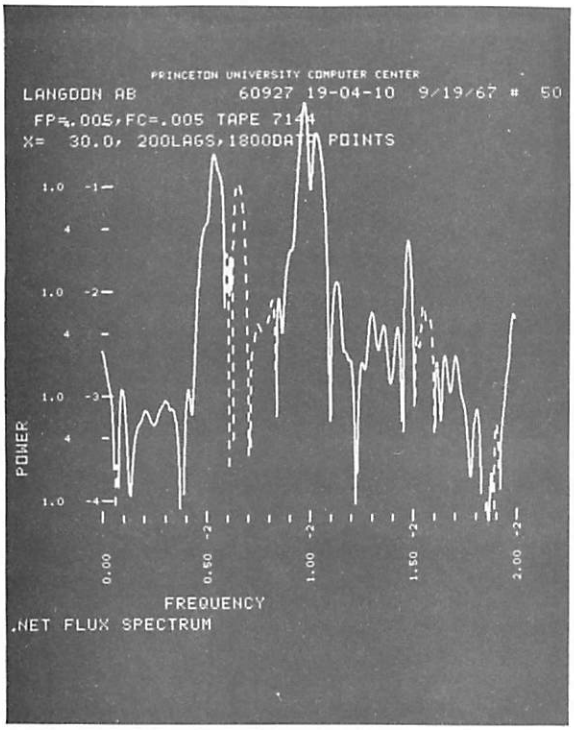

(g) X = 30

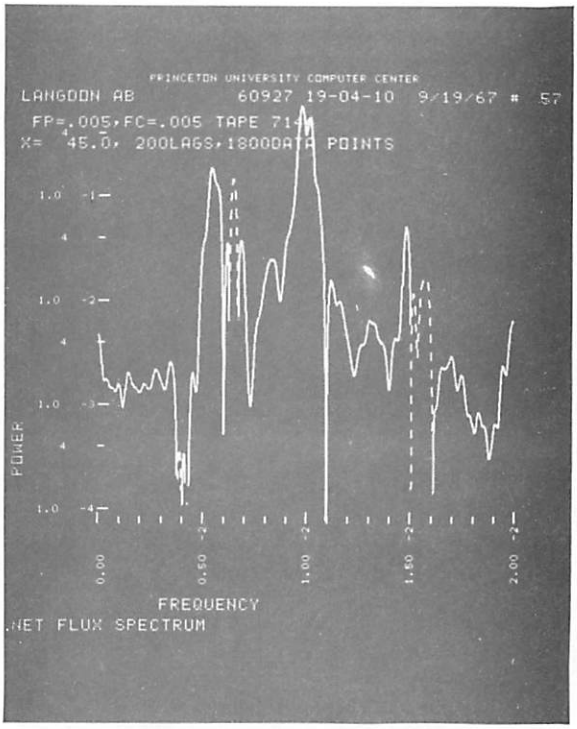

(h) X = 45

(continued next page)

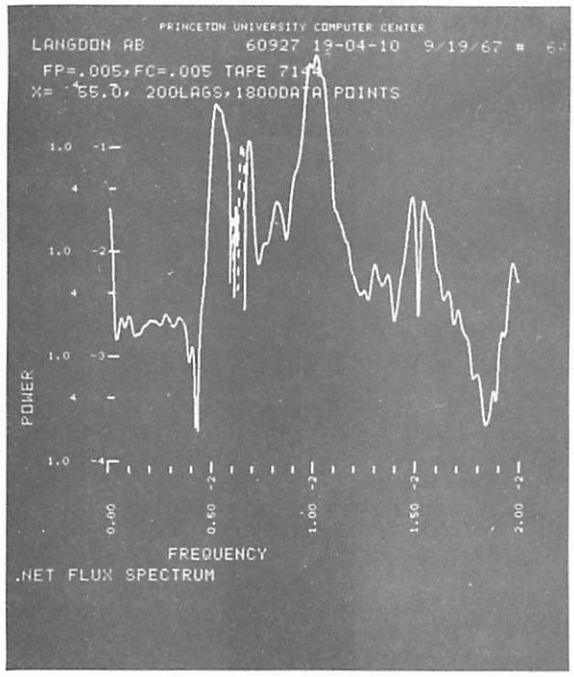

(i) X = 55

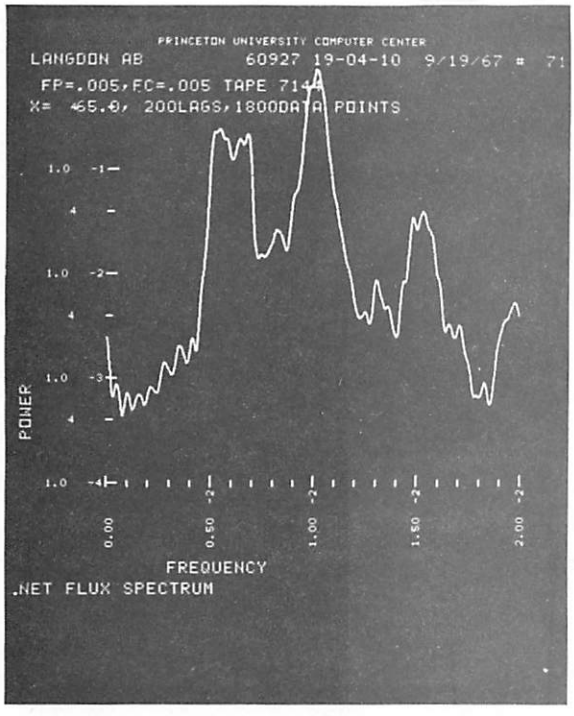

(j) X = 65

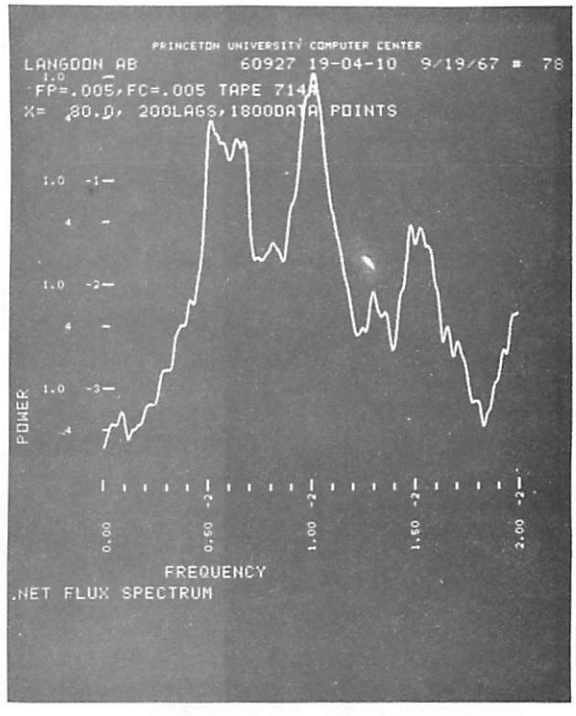

(k) X = 80

Fig. V. 3. Poynting flux spectrum

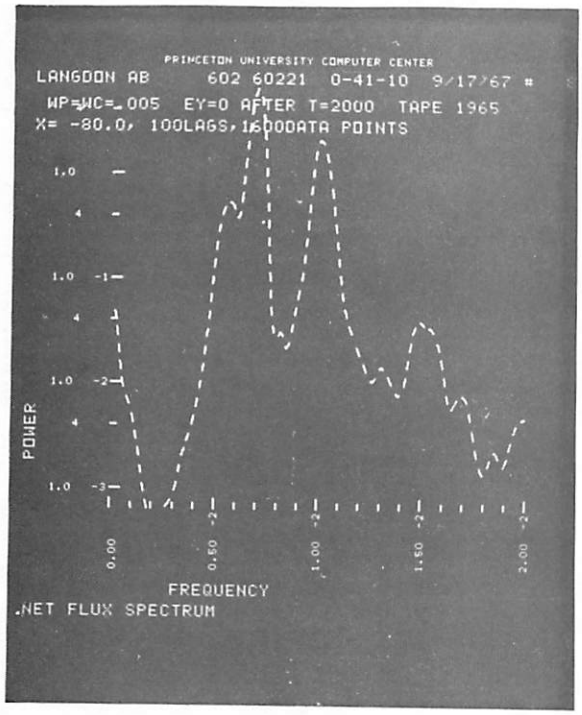

(a) X = - 80

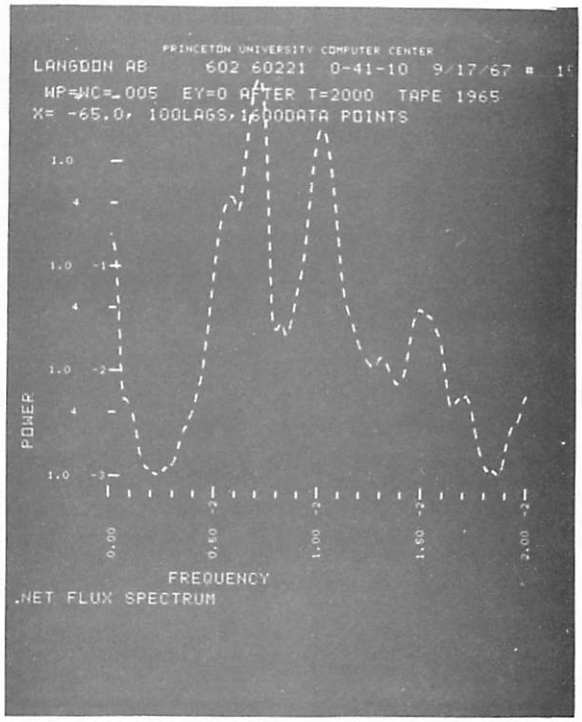

(b) X = -65

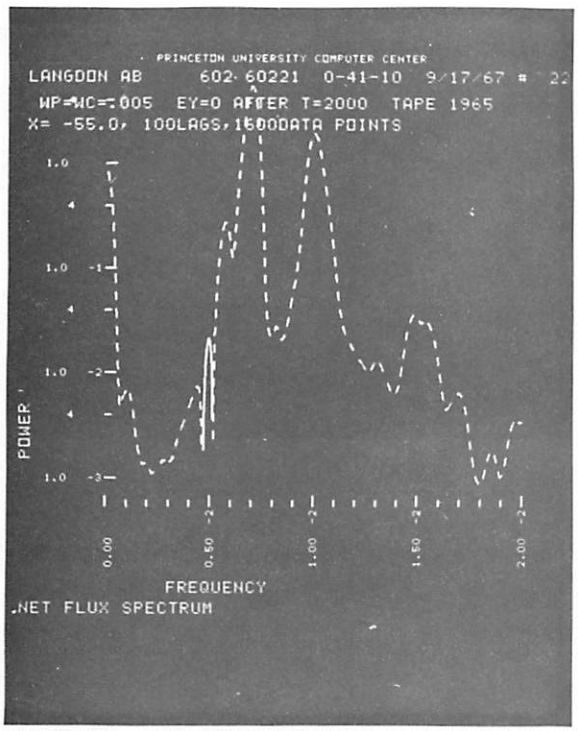

(c) X = - 55

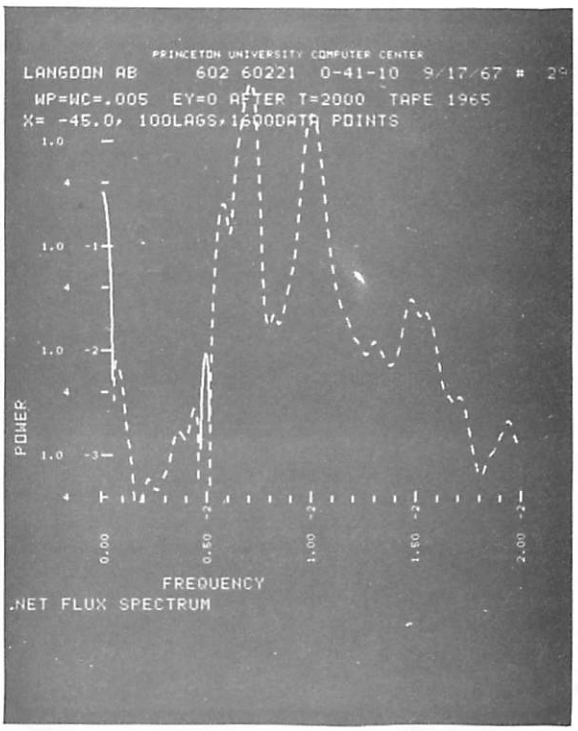

(d) X = - 45

(continued next page)

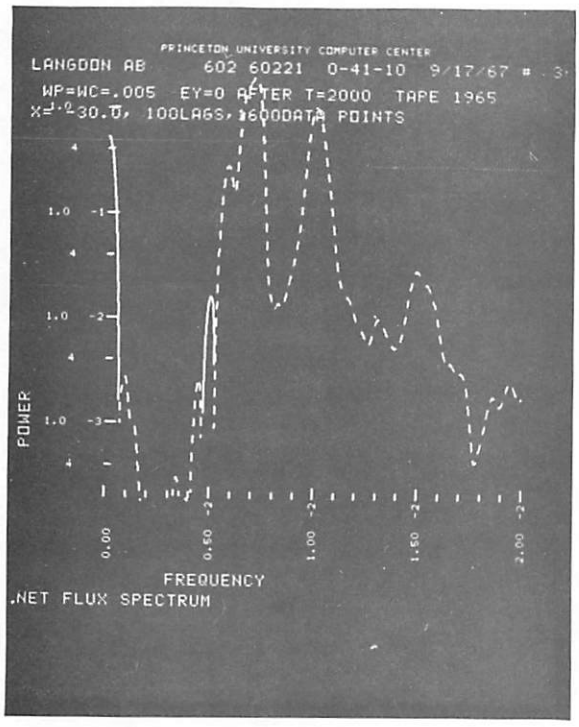

(e) X = -30

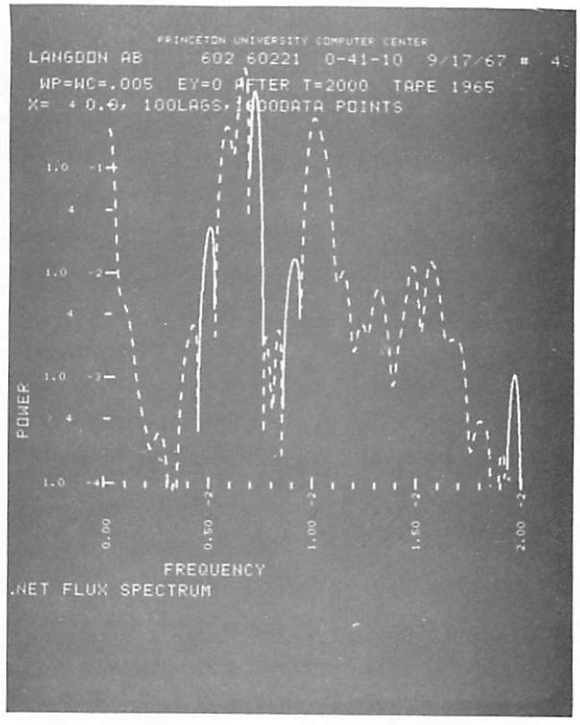

(f) X = 0

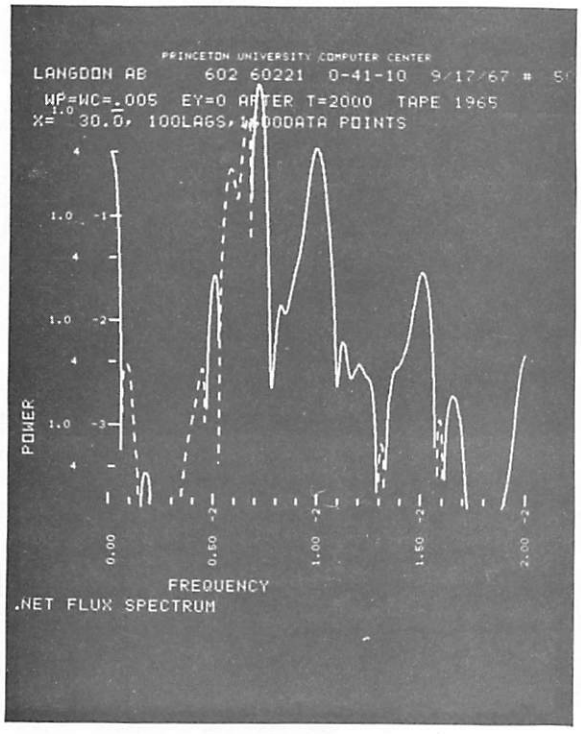

(g) X = 30

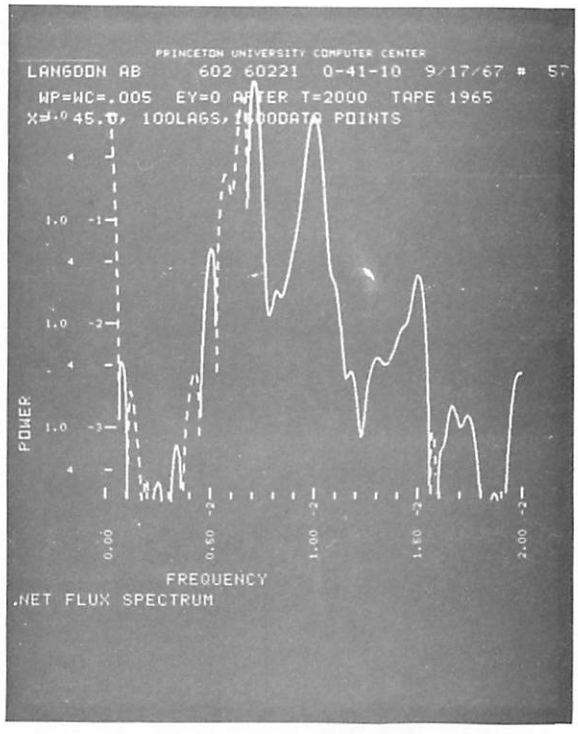

(h) X = 45

(continued next page)

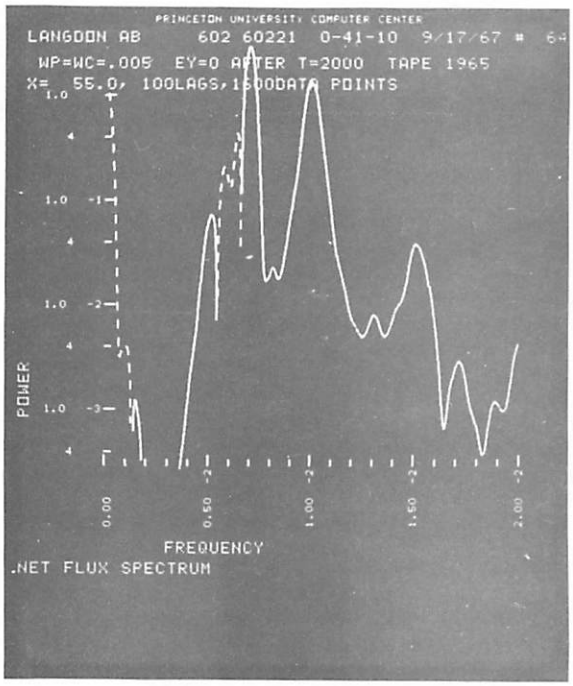

(i) X = 55

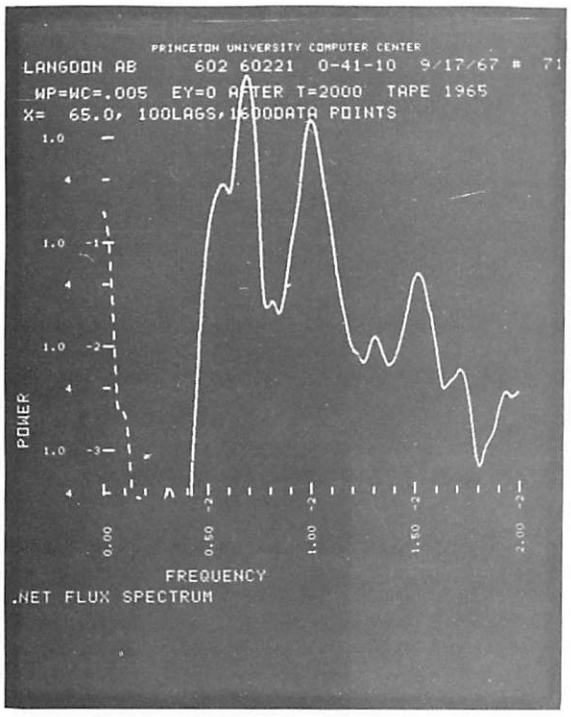

(j) X = 65

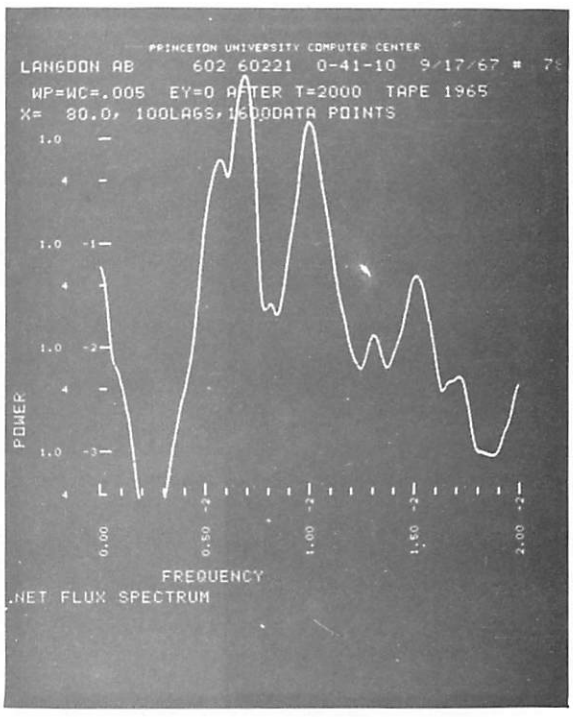

(k) X = 80

Fig. V. 4. Poynting flux spectrum